STATE RESEARCH CENTER OF RUSSIA

INSTITUTE FOR HIGH ENERGY PHYSICS

NuMI–B–471

February 15, 1999

The PH2M Two Horns Focusing System for the NuMI Project

(Task A Report of the Accord between FNAL and IHEP)

V.Garkusha, F.Novoskoltsev, V.Zarucheisky

Protvino 1999

Contents

1 PH2M Focusing System for the NuMI Project

The two horns focusing system PH2 with parabolic shaped inner conductors has been developed for the NuMI Project [1]. This focusing system provides in three steps wide band neutrino beams in the energy range from 1 GeV up to 25 GeV. Corresponding WBB designs for the low energy (1–6 GeV), medium energy (2–12 GeV) and high energy (5–25 GeV) ranges use the same horns and power supply system, although with different targets and the second horn in different positions, as it is shown in Figure 1.1. Two of these configurations (ME and HE) provide neutrino beams with the energy higher then the threshold of the τ-lepton production. Proposed neutrino beam optics design with addition of some dipoles, collimators and a primary proton beam absorber allows to have also narrow band beams with the parent particle momenta from 10 GeV/c up to 45 GeV/c.

The shapes of PH2 horn inner conductors have been initially optimized for producing of neutrino beams in the ME range. LE and HE neutrino beam configurations result from the optimization of horn locations and target parameters only. In particular, the 0.8 m long beryllium and 0.94 m long graphite rod targets were proposed for LE and ME beam configurations respectively, while the 1.6 m long graphite or beryllium fin target with average density reduced by air gaps between target segments ($\leq$0.64 of nominal material density) was designed for the HE beam configuration.

Variations of a target location for each configuration allow to obtain neutrino beams with energy spectra different from spectra shown in Figure 1.1. One should note, that in their present state LE and ME configurations provide neutrino beams with lowest average energy, which may be produced using these horns with a target located inside and outside the first horn respectively. On the contrary, the HE configuration gives practically the highest average energy neutrino beam, which may be obtained with help of this horns in the 50 m long target hall.

This Section presents results of additional optimization of the shapes of PH2 horn inner conductors, which was performed in order to:

- increase the neutrino event rate for the LE beam without substantial loss of it for ME and HE neutrino beams;

[1] Main results of beam optics and target designs are described in Task B and C IHEP Reports, NuMI–B–394, NuMI–B–454, 1998 and in the NuMI Facility Technical Design Report, October 1998.

- provide the possibility of using in the case of the baseline ME beam configuration of the more longer fin target with average density $\leq$0.8 of nominal material density, as well as the solid rod target.

The first item allows us to improve the MINOS sensitivity to neutrino oscillations in the region of small Δm^2, while the second one provides to use the same target design for both ME and HE beams. Main parameters of this new optics design (labeled as PH2M) and resulting neutrino spectra are given below.

1.1 Modifications in the Shape of Inner Conductors with Respect to the Original Design

Figure 1.2 shows the shapes of new PH2M inner conductors in comparison with those for the original PH2 design. Numerical description of new inner conductors are given in Tables 1.1 and 1.2; optimized layouts of different beam configurations of the PH2M design — in Table 1.3.

In this new inner conductor design the larger final radius of the downstream parabola in the first horn will provide more effective focusing of the low energy parent mesons in the LE beam configuration, while the shorter length of the neck region compensates the displacement of the effective center for the smaller density (and consequently more longer) fin target upstream the proton beam in the ME beam configuration. Non–symmetric shape of the inner conductor in the second horn will provide more neutrinos with E_ν = 2.5–4.5 GeV at the far detector for the LE beam configuration, while the larger neck radius simplifies the baffle protection system in the case of the HE beam configuration.

Modifications in the shape of PH2 horn inner conductors were followed by changes in the depth of focus for all neutrino beam configurations as it is shown in Figure 1.3. These curves were obtained by neutrino event rate calculations at the far detector for different locations of the point–like target with respect to the upstream end of the first horn and are thus normalized that 1.0 is the highest point of each curve. Depths of the focus in all configurations of the PH2M focusing system (as it follows from these plots) are wider with respect to those in the original PH2 design and are dislodged upstream the proton beam. It means, that in the case of the PH2M design:

- besides of beryllium target, the longer graphite target may also be used for the LE beam configuration [2]. Both targets should be located 0.2–0.3 m upstream with respect to the target in the PH2 design;

- the fin target with average density reduced by air gaps between teeth may be used for the ME beam configuration, as well as more dense rod target which has been used for the PH2 design;

- the same as in the PH2 design the 1.6 m long fin target, moved 0.6–1.0 m upstream the proton beam, may be used for the HE beam configuration.

1.2 Neutrino Event Rates at the Far Detector

The results of neutrino beam simulations at the far detector for the focusing system with new PH2M horns in comparison with those for the original PH2 design are given in Figures 1.4–1.6 and Tables 1.4–1.6 respectively. Calculations have been made using the Fermilab GEANT based software GNuMI for three (LE, ME and HE) neutrino beams. The total length of the decay region is equal to 725 m (675 m is the length of the decay pipe and 50 m is a distance between the target and the upstream end of the decay pipe) [3]. Main parameters of targets, which have been used in these calculations are given in Table 1.3. The proton beam had Gaussian distributions in both horizontal and vertical planes with $\sigma_x = \sigma_y = r/2.25$ for graphite and beryllium rod targets with radius r and $\sigma_x = 0.71\,\mathrm{mm}$, $\sigma_y = 1.42\,\mathrm{mm}$ for graphite fin targets.

As it follows from results of neutrino beam simulations, in the case of the LE beam configuration new PH2M horns give with respect to the original PH2 design 11% increase in the ν_μ CC event rate for neutrino with $E_\nu < 6$ GeV. Two interaction lengths graphite target, which may be successfully used here due to the wider depth of the focus, allows to obtain substantially more (factor 1.4) neutrino events with E_ν = 3–6 GeV than two interaction lengths beryllium target. Changes in the shape of inner conductors do not influence on the neutrino event rate in the energy range of $E_\nu < 3$ GeV for both beryllium and graphite targets.

[2] Preliminary results of the LE target conceptual design show, that graphite rod target, as well as beryllium one, may be considered for this neutrino beam configuration.

[3] Neutrino spectra for the original PH2 design shown in Figure 1.1 have been calculated for the 800 m long decay region.

For ME and HE beam configurations the use of new PH2M horns leads to 6–8% decrease in the total ν_μ CC event rate, while the total ν_τ CC event rate (for $\Delta m^2 = 0.001\,\mathrm{eV}^2$ and $\sin^2 2\theta = 1$) in the case of the HE beam configuration remains almost without changes. The loss of the total ν_μ CC event rate in the case of the HE beam configuration follows directly from decreasing of the area filled by focusing magnetic field in the vicinity of the beam axis (due to shortening of the neck region in the first horn and the larger neck radius in the second one).

1.3 Conclusions

Besides of changes in neutrino spectra, which properly reflect the aims of additional optimization of PH2 horn inner conductors, new shapes of inner conductors in PH2M horns give also the following practical advantages:

1. New shape of the inner conductor in the first horn allows to have significantly more space in transverse direction for a target module in the LE beam configuration (in this case the target extends 0.60 m inside the first horn where the radius of its inner conductor is equal to 1.9 cm, while for the original PH2 design the target extends up to the horn neck region where available space is only 0.95 cm in radius).

2. Shorter neck region of the inner conductor in the first horn (0.04 m instead of 0.15 m) may reduce heating and stresses in the inner conductor.

3. Larger neck radius of the inner conductor in the second horn (4 cm instead of 3 cm) simplifies design of a baffle protection system in the case of HE beam configuration.

One should also note, that as in the case of the original PH2 design, new PH2M horns may be used for producing of a narrow band neutrino beam over a wide range of neutrino energies.

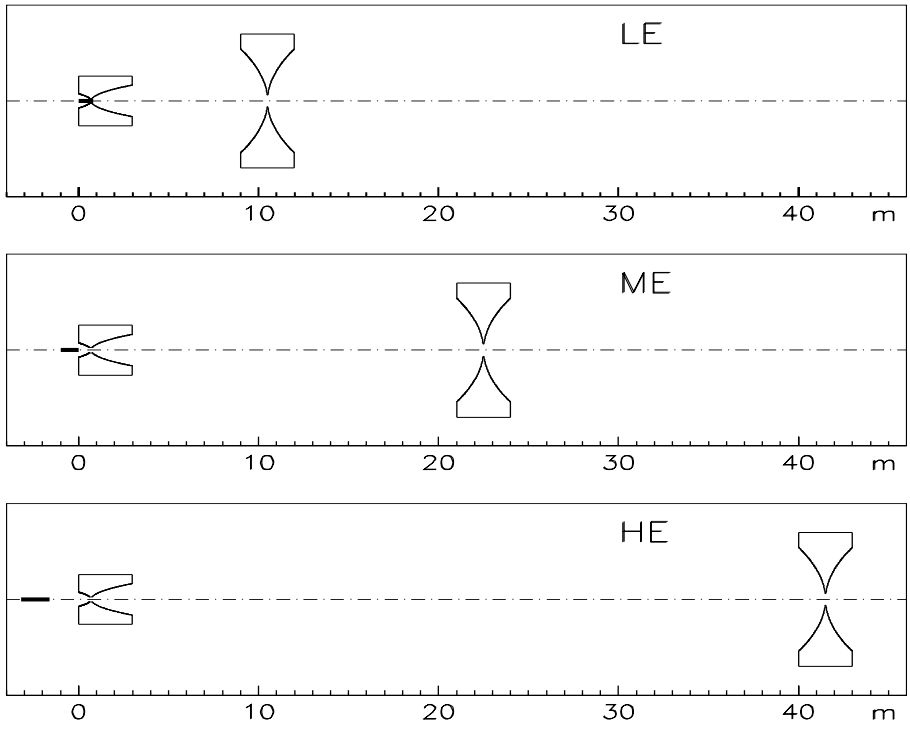

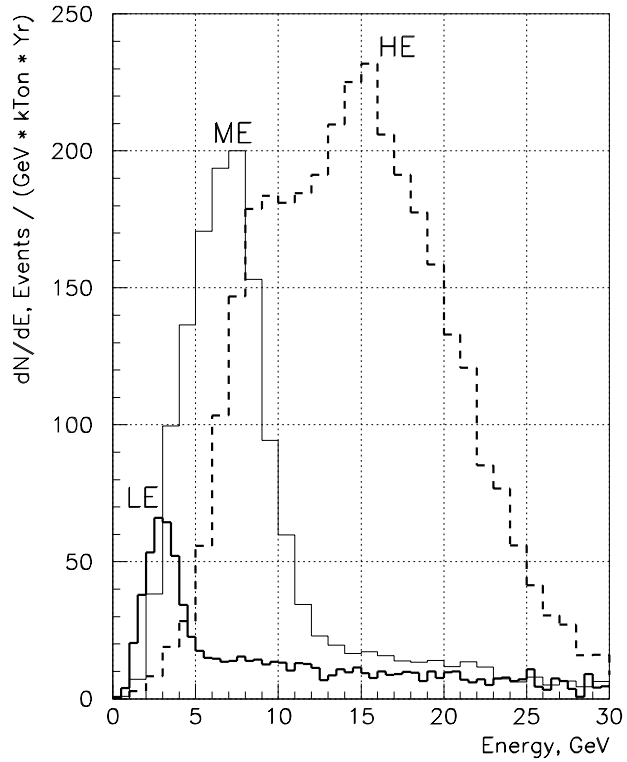

Figure 1.1: Layouts and corresponding spectra of ν_μ CC events at the far detector for three different configurations of the PH2 design.

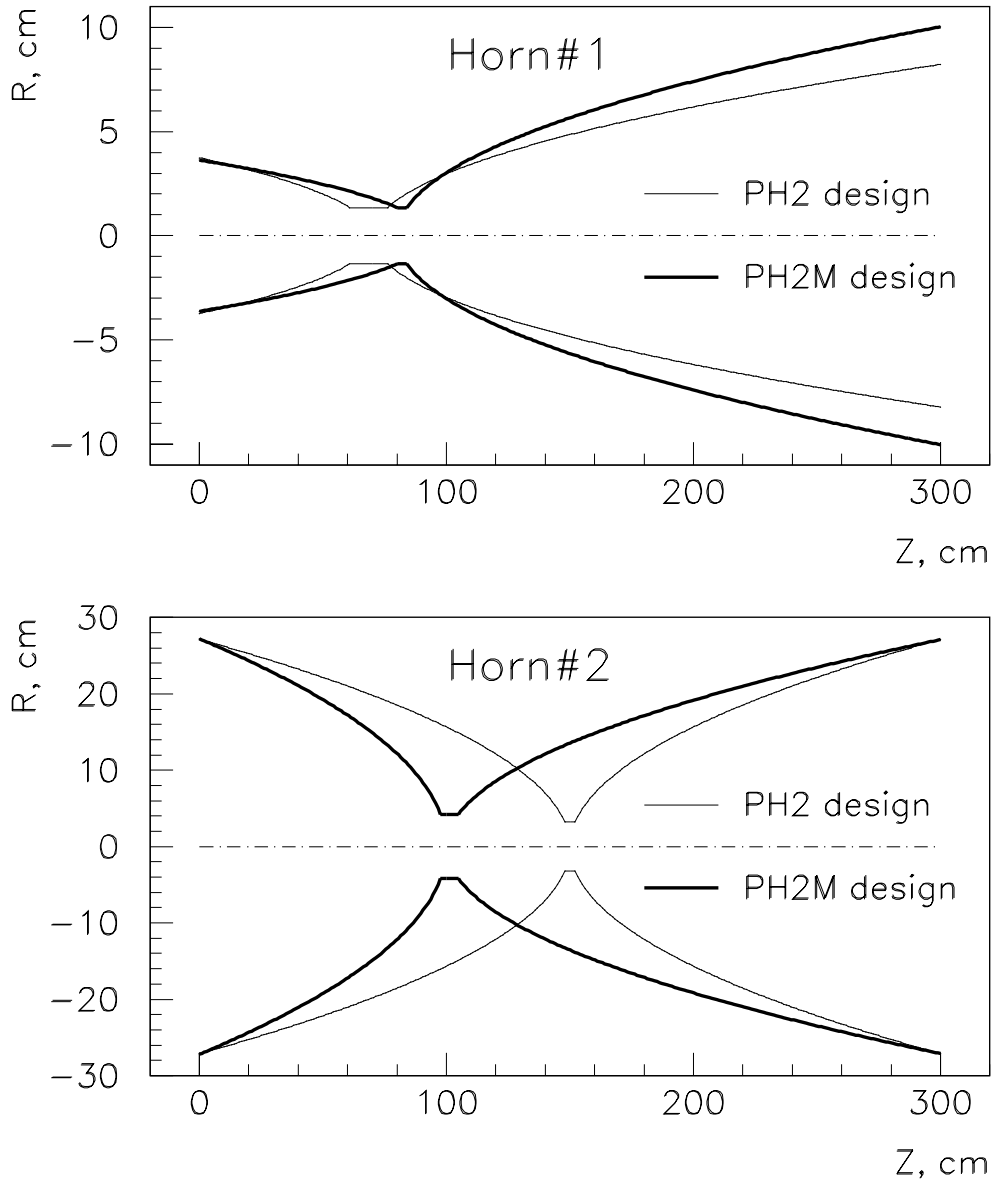

Figure 1.2: Shapes of PH2M horn inner conductors in comparison with those for the original PH2 design.

Horn#1	Upstream		Neck	Downstream	
Z, cm	0.–44.047	44.047–80.	80.–83.982	83.982–95.128	95.128–300.
R_{in}^{IC}, cm	$\sqrt{\frac{92.8454-Z}{7.0483}}-0.2$	$\sqrt{\frac{85.7091-Z}{7.0483}}$	0.90	$\sqrt{\frac{Z-82.2123}{2.1850}}$	$\sqrt{\frac{Z-80.}{2.1850}}-0.2$
R_{out}^{IC}, cm	$\sqrt{\frac{92.8454-Z}{7.0483}}$		1.35	$\sqrt{\frac{Z-80.}{2.1850}}$	
R_{in}^{OC}, cm	15.33				
R_{out}^{OC}, cm	16.20				

Table 1.1: Horn 1 of the PH2M design. Z=0 is the upstream end of the horn. IC stands for the inner conductor, OC for the outer conductor.

Horn#2	Upstream	Neck	Downstream
Z, cm	0.–97.617	97.617–104.803	104.803–300.
R_{in}^{IC}, cm	$\sqrt{\frac{100.-Z}{0.1351}}-0.2$	4.00	$\sqrt{\frac{Z-100.}{0.2723}}-0.2$
R_{out}^{IC}, cm	$\sqrt{\frac{100.-Z}{0.1351}}$	4.20	$\sqrt{\frac{Z-100.}{0.2723}}$
R_{in}^{OC}, cm	37.00		
R_{out}^{OC}, cm	37.87		

Table 1.2: Horn 2 of the PH2M design. Z=0 is the upstream end of the horn. IC stands for the inner conductor, OC for the outer conductor.

	LE–beam		**ME–beam**	**HE–beam**
Target				
$Z_{upstream}$	–0.2 m	–0.34 m	–1.3 m	–4.0 m
$Z_{downstream}$	0.6 m	0.6 m	–0.1 m	–2.4 m
Material–Shape	Be–rod	C-rod	C–fin	C–fin
Length	0.8 m	0.94 m	1.2 m	1.6 m
Average density	1.82 g/cm^3	1.81 g/cm^3	1.42 g/cm^3	1.16 g/cm^3
Diameter (Thickness)	6.4 mm	4.0 mm	3.2 mm	3.2 mm
Horn#1				
$Z_{upstream}$	0.0 m		0.0 m	0.0 m
$Z_{downstream}$	3.0 m		3.0 m	3.0 m
Horn#2				
$Z_{upstream}$	10.0 m		23.0 m	40.0 m
$Z_{downstream}$	13.0 m		26.0 m	43.0 m

Table 1.3: Layouts for different configurations of the PH2M design.

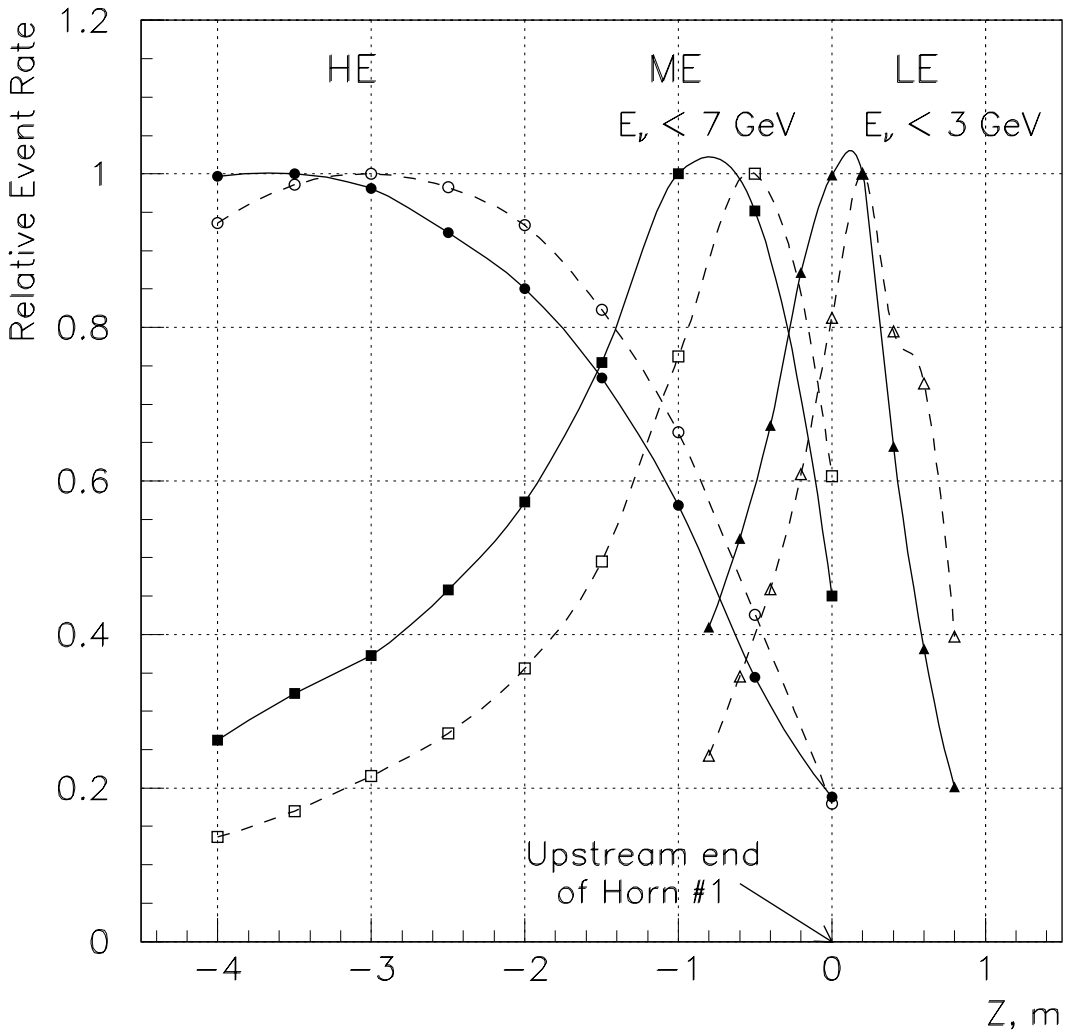

Figure 1.3: Depths of the focus for PH2M neutrino beam configurations (solid lines) in comparison with those for the original PH2 design (dashed lines).

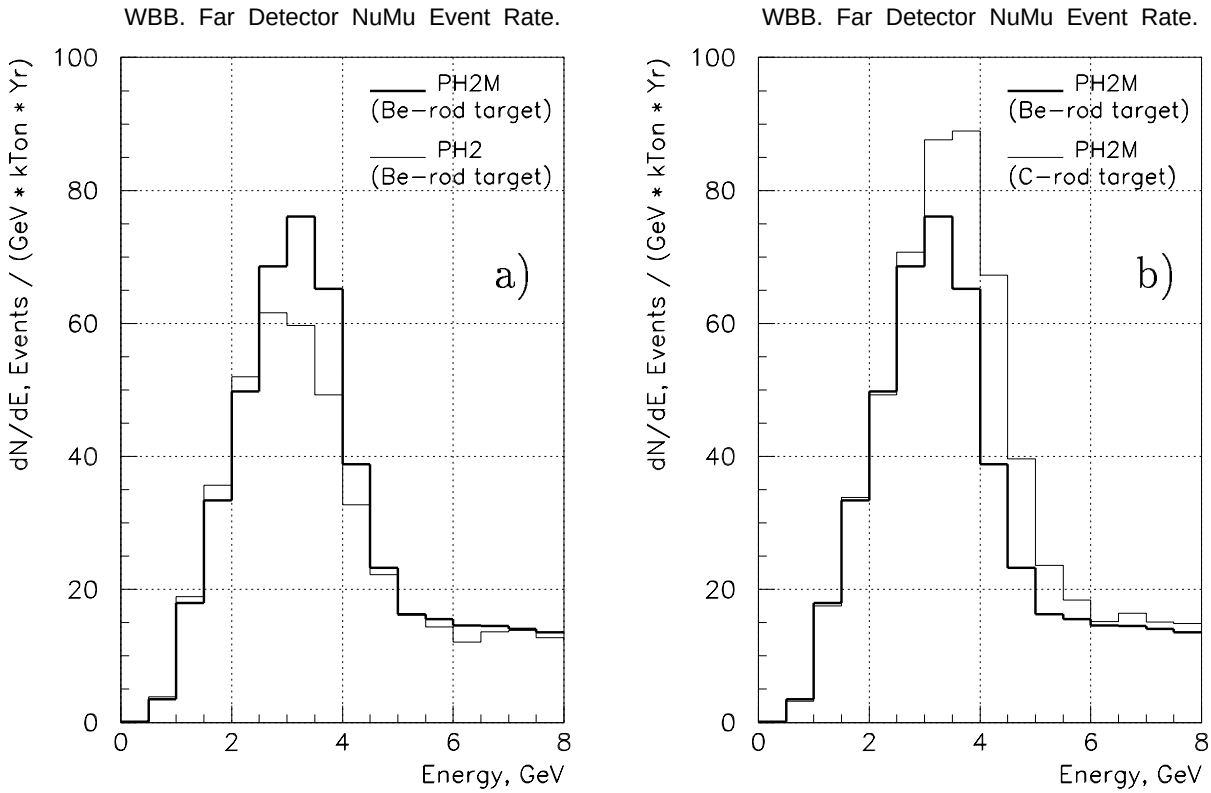

Figure 1.4: The LE neutrino beam. Energy spectrum of ν_μ CC events at the far detector for the PH2M design in comparison with that for the original PH2 design (a) and energy spectra for the PH2M design with different targets (b).

	Number of ν_μ CC events per kTon·Yr			GNuMI outputs
Design/Target	0–3 GeV	0–6 GeV	Total	in:
PH2 /Be-rod	86	183	426	job111–112
PH2M/Be-rod	87	204	434	job131–132
PH2M/C-rod	87	250	461	job141–142

Table 1.4: Event rates at the far detector for different LE beam designs. GNuMI outputs are located in the /usr/minos/date01/ihep/le_wbb/ file area.

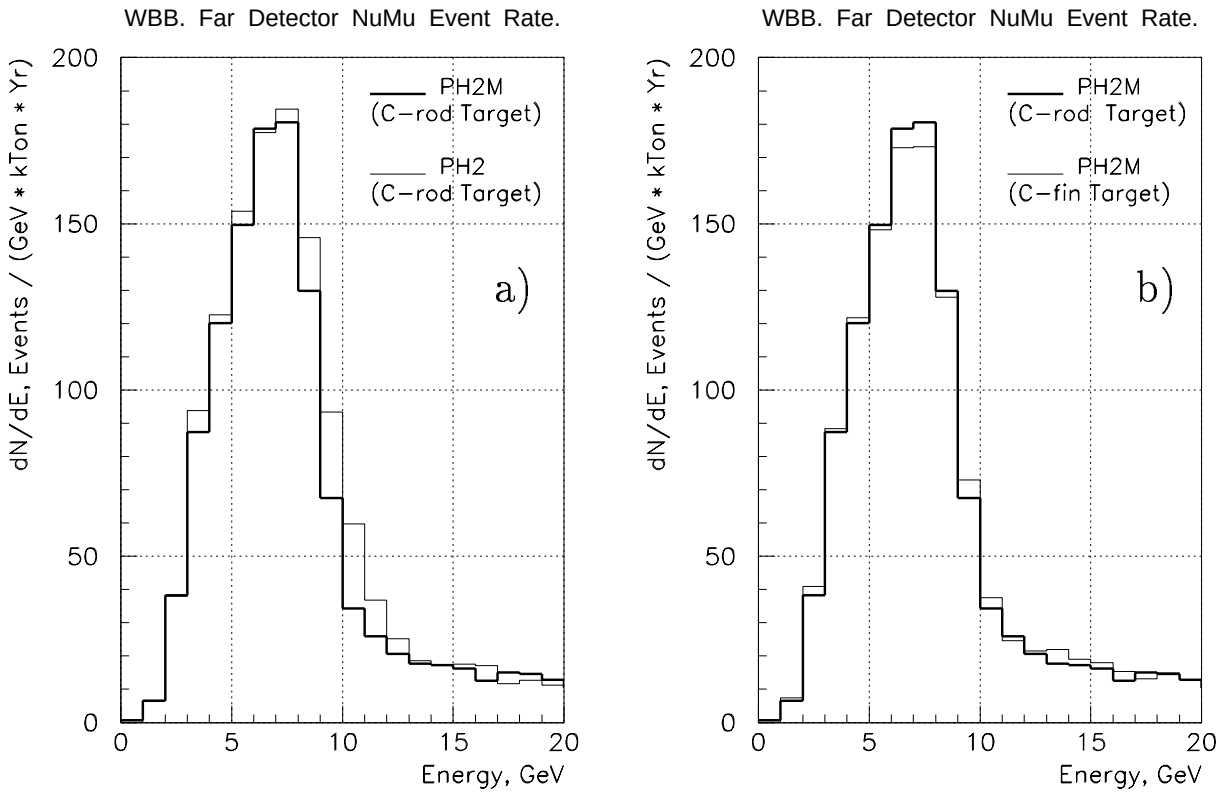

Figure 1.5: The ME neutrino beam. Energy spectrum of ν_μ CC events at the far detector for the PH2M design in comparison with that for the original PH2 design (a) and energy spectra for the PH2M design with different targets (b).

	Number of ν_μ CC events per kTon·Yr			GNuMI outputs
Design/Target	0–6 GeV	0–12 GeV	Total	in:
PH2 /C-rod	416	1114	1367	job87–90
PH2M/C-rod	403	1020	1262	job75–78
PH2M/C-fin	408	1016	1277	job71–74

Table 1.5: Event rates at the far detector for different ME beam designs. GNuMI outputs are located in the /usr/minos/date01/ihep/me_wbb/ file area.

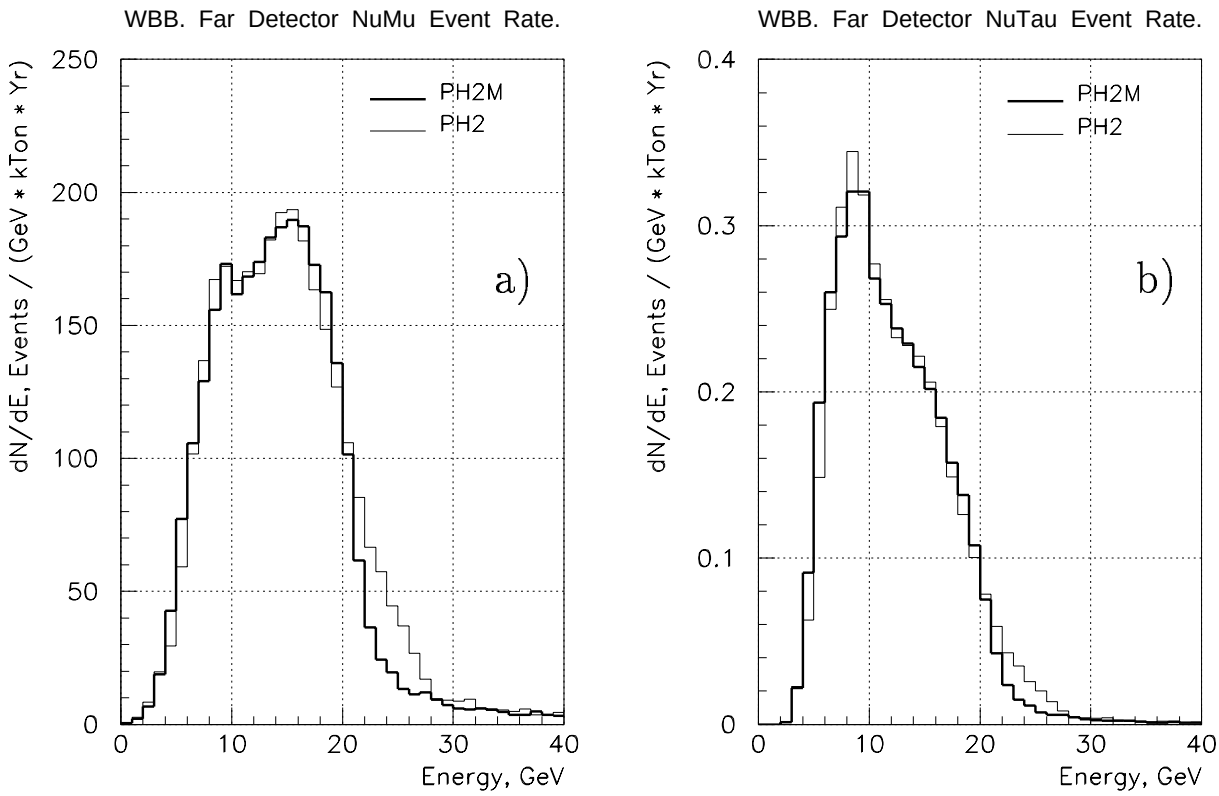

Figure 1.6: The HE neutrino beam. Energy spectra at the far detector of ν_μ CC events (a) and ν_τ CC events ($\Delta m^2 = 0.001\,\mathrm{eV}^2$, $\sin^2 2\theta = 1$) (b) for the PH2M design in comparison with those for the original PH2 design.

	Number of CC events per kTon·Yr		GNuMI outputs
Design/Target	ν_μ	ν_τ	in:
PH2 /C-fin	2995	3.76	job59–62
PH2M/C-fin	2823	3.71	job51–54

Table 1.6: ν_μ and ν_τ ($\Delta m^2 = 0.001\,\mathrm{eV}^2$, $\sin^2 2\theta = 1$) event rates at the far detector for different HE beam designs. GNuMI outputs are located in the /usr/minos/date01/ihep/le_wbb/ file area.

2 Thickness of PH2M Horn Inner Conductors

Secondary particles are focusing in horns by toroidal magnetic field located in the volume between inner and outer conductors of the horn. To enter into the field region and to leave it, secondaries pass through horn inner conductors, which have to be as thin as possible to minimize the absorption losses. On the other hand, inner conductors of the horns should be thick enough to carry out 200 kA pulsed current. Because the thickness of inner conductors in horns is a result of a compromise between small losses of secondaries and high reliability of mechanical design, the dependence of the neutrino event rate on the inner conductor thickness was investigated for all configurations of the PH2M focusing system.

Calculations have been made using the M. C. program HALO for modified horns of the PH2M design and for the 725 m long decay region. Absorption and scattering, as well as focusing of secondaries inside the inner conductor walls were taken into account. Graphite fin targets with average density 0.78 and 0.64 of nominal graphite density were used in neutrino flux simulations for ME and HE beam configurations respectively (corresponding target lengths were equal to 1.2 m and 1.6 m), while the 0.8 m long beryllium rod target was used in the case of the LE beam configuration.

2.1 Nominal Thickness

In the PH2M design the thickness of the inner conductor in the first horn increases continuously from 2 mm near flanges up to 4.5 mm in the neck region. The thickness of the inner conductor in the second horn is constant along the whole length and is equal to 2 mm. At these values of nominal thicknesses of PH2M horn inner conductors, the losses of the ν_μ CC event rate at the far detector due to the absorption in the inner conductor material are equal to 16–17% for the whole neutrino spectrum in ME and HE beam configurations and for neutrino with $E_\nu < 6$ GeV in the LE beam configuration. Total absorption losses of the ν_μ CC event rate in the LE beam are equal to 12%. Approximately 2–3% decrease of the ν_μ CC event rate for all neutrino beams gives also multiple Coulomb scattering of secondaries in the material of inner conductors.

The ν_μ CC event rates at the far detector as functions of the inner conductor radius R_{in}^{IC}, where pions contributing to this neutrino event rate

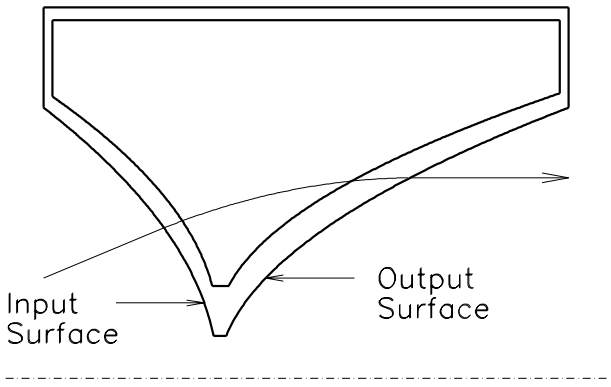

cross the inner conductor, are given in Figures 2.1–2.3 for three different neutrino beams in the case of nominal thicknesses of inner conductors. The maximum difference between distributions of "useful" pions at input and output surfaces of the inner conductor occurs for the first horn in the LE beam configuration. This difference, which is a natural feature of the LE focusing system, reduces in the first horn in ME and HE beam configurations and is negligible in the second horn in all configurations of the PH2M design.

As it follows from these plots, in LE and ME beam configurations almost the total number of neutrino events arises from pions which cross inner conductor walls of the first horn through its parabolic shaped parts with radii 0.9–3.4 cm and 0.9–9.8 cm for input and output surfaces respectively. The radius in the most important part of the inner conductor for the second horn varies from 5 cm up to 20 cm, which corresponds to the 1.5 m in length part of the conductor with Z = 45–210 cm from the upstream end of the horn.

One should note, that given results show not quite optimum use of PH2M horns in the case of the HE beam configuration, i.e.:

- approximately one half of neutrino events arises from pions which enter the field region of the first horn crossing the inner conductor under its parabolic shaped part,
- only the central part of the second horn inner conductor "works" effectively for producing of the neutrino flux at the detector,

which follows from their initial optimization for producing of neutrino beams in the low energy range and inadequate length of the target hall.

2.2 Larger Thickness

Because a noticeable decrease of inner conductor thicknesses looks as not quite real then taking into account preliminary horn fatigue analysis given in the NuMI Facility Technical Design Report (October 1998), this Section gives results of calculations showing the effects on neutrino energy spectra with increasing of inner conductor thicknesses. There are two possible ways to increase the thickness of horn inner conductor:

- keeping the outer surface of inner conductors unchanged and increasing the thickness towards the horn axis ("inside"),
- keeping the inner surface of inner conductors unchanged and increasing the thickness from the horn axis ("outside").

Due to different distributions of the magnetic field inside and outside of inner conductors, these two ways will give different changes in neutrino energy spectra.

2.2.1 Double "inside" Thickness

Figure 2.4 illustrates the effects of double thicknesses of inner conductors, which were increased "inside"[4], on the neutrino energy spectrum at the far detector for the baseline ME configuration. As it follows from these plots, doubling of a thickness of the inner conductor in the second horn does not effect noticeable on the neutrino event rate at the far detector. Otherwise, doubling of the inner conductor thickness in the first horn leads to the 10% decrease of the event rate in the energy range of $E_\nu < 8.7$ GeV and to the 22% event rate increase in the energy range of $E_\nu > 8.7$ GeV. The total neutrino event rate is about 2.5% less than that in the case of the nominal thickness of the first horn inner conductor. The increase of the neutrino event rate in the energy range of $E_\nu > 8.7$ GeV is provided by additional focusing (by magnetic field inside thick neck) of 20–40 GeV/c pions, which are passing through the hole in the first horn in the case of the nominal inner conductor thickness.

Figures 2.5, which gives neutrino event rates as functions of the inner conductor radius, where pions contributing to this neutrino event rate cross the inner conductor, shows that decrease of the neutrino event rate in the

[4]In this case the first horn has only 4.5 mm radius of the hole for primary proton passing.

energy range of $E_\nu > 8.7$ GeV occurs mainly due to extra absorption of pions in the inner conductor material at radii larger than 2.0 cm.

Similar calculations performed for other neutrino beam configurations show that double "inside" thickness of the first horn inner conductor leads to following (with respect to its nominal thickness) changes in neutrino event rates at the far detector (see also Figure 2.8):

- 8% decrease for neutrino with $E_\nu < 3.8$ GeV, 9% increase for neutrino with $E_\nu > 3.8$ GeV and nearly the same total event rate for the LE beam,
- 12% decrease for neutrino with $E_\nu < 20.3$ GeV, 37% increase for neutrino with $E_\nu > 20.3$ GeV and 9% decrease of the total event rate for the HE beam.

2.2.2 Double "outside" Thickness

The effects on the neutrino spectrum are determined in this case not only by larger absorption and scattering of secondaries and by small changes of their focusing inside the inner conductor material, as it takes place when the thickness is increased "inside". The considerable effect occurs here also due to decreasing of the area filled by focusing magnetic field and decreasing of the field value in the outer surface of the inner conductor.

Figure 2.6 illustrates the effects of double thicknesses of inner conductors, which were increased "outside", on the neutrino energy spectrum at the far detector for the baseline ME configuration. Double thickness of the inner conductor in the first horn gives in this case the considerable loss of the neutrino event rate in all energy range covered by this neutrino beam. As in the previous case, decreasing of the neutrino event rate due to double thickness of the inner conductor in the second horn is smaller than that in the first horn, but contrary to increasing of the thickness "inside" its value should not be neglected. Figures 2.7 illustrates this loss as function of the inner conductor radius in the first horn, where pions contributing to this neutrino event rate cross the inner conductor.

The decrease of the total event rate at the far detector due to double "outside" thickness of inner conductors in PH2M horns with respect to the nominal event rate is given in Table 2.1 for all neutrino beam configurations (see also Figure 2.8).

Horn	Neutrino event rate decrease in the energy range of (GeV):				
	LE–beam		ME–beam		HE–beam
	< 6	< 100	< 12	< 100	< 100
horn#1	28%	16%	29%	21%	17%
horn#2	9%	6%	8%	7%	5%

Table 2.1: The decrease of the total event rate at the far detector due to double "outside" thickness of inner conductors in PH2M horns.

2.2.3 FAR/NEAR Ratio

The effects of larger inner conductor thicknesses on the FAR/NEAR ratio, which would be used to predict the neutrino flux at the far detector, are described here by deviation from 1.0 the value of RR, defined as:

$$RR = \frac{FAR(t)/NEAR(t)}{FAR(0)/NEAR(0)},$$

where FAR(0), NEAR(0), FAR(t) and NEAR(t) are neutrino energy spectra at the center of far and near detectors for nominal (0) and changing (t) thicknesses of horn inner conductors respectively. It was assumed, that the near detector is located 300 m beyond the end of the decay pipe.

Figure 2.9 shows deviations of RR from 1.0 calculated in the case of double thickness of the inner conductor in the first horn for different configurations of the PH2M focusing system. As it follows from these plots, maximum deviation of the FAR/NEAR ratio from its nominal value (40–60%) is reached for the HE beam configuration, when the LE beam configuration is more less sensitive to changing in thickness of the inner conductor in the first horn from the point of view of minimal changes of the FAR/NEAR ratio. The deviation of the FAR/NEAR ratio from its nominal value does not exceed here 15%.

In all configurations of the PH2M focusing system the deviation of RR from 1.0 due to the larger inner conductor thickness takes place for neutrinos with the energy greater than average value for corresponding neutrino energy spectrum. This behavior of RR as function of energy is similar to that which occurs in the case when horns and target are missaligned (see Figures 3–6–3 and 3–6–6 of the NuMI Facility Technical Design Report, October 1998), and may be explained by the fact that the main contribution

to the low energy half of neutrino spectrum arises from decays of parent mesons with large angles between the parents direction and the direction of a neutrino. Small changes in focusing of these parents (following from changing in thickness of inner conductors) does not effect considerably on the FAR/NEAR ratio.

2.3 Conclusions

The results of calculations described above show, that:

1. The effects on neutrino spectra at the far detector on variations of a thickness of horn inner conductors are considerably different for first and second horns of the PH2M design, i.e. the influence of the thickness of the inner conductor in the second horn on the neutrino event rate is rather smaller than that in the first horn.

2. For both horns increasing of the thickness towards the horn axis ("inside") is more preferable than increasing from the horn axis ("outside") from the point of view of minimal additional losses of neutrinos. Moreover, an increase of the thickness "inside" in the neck region of the inner conductor gives a some increase of the event rate at the detector.

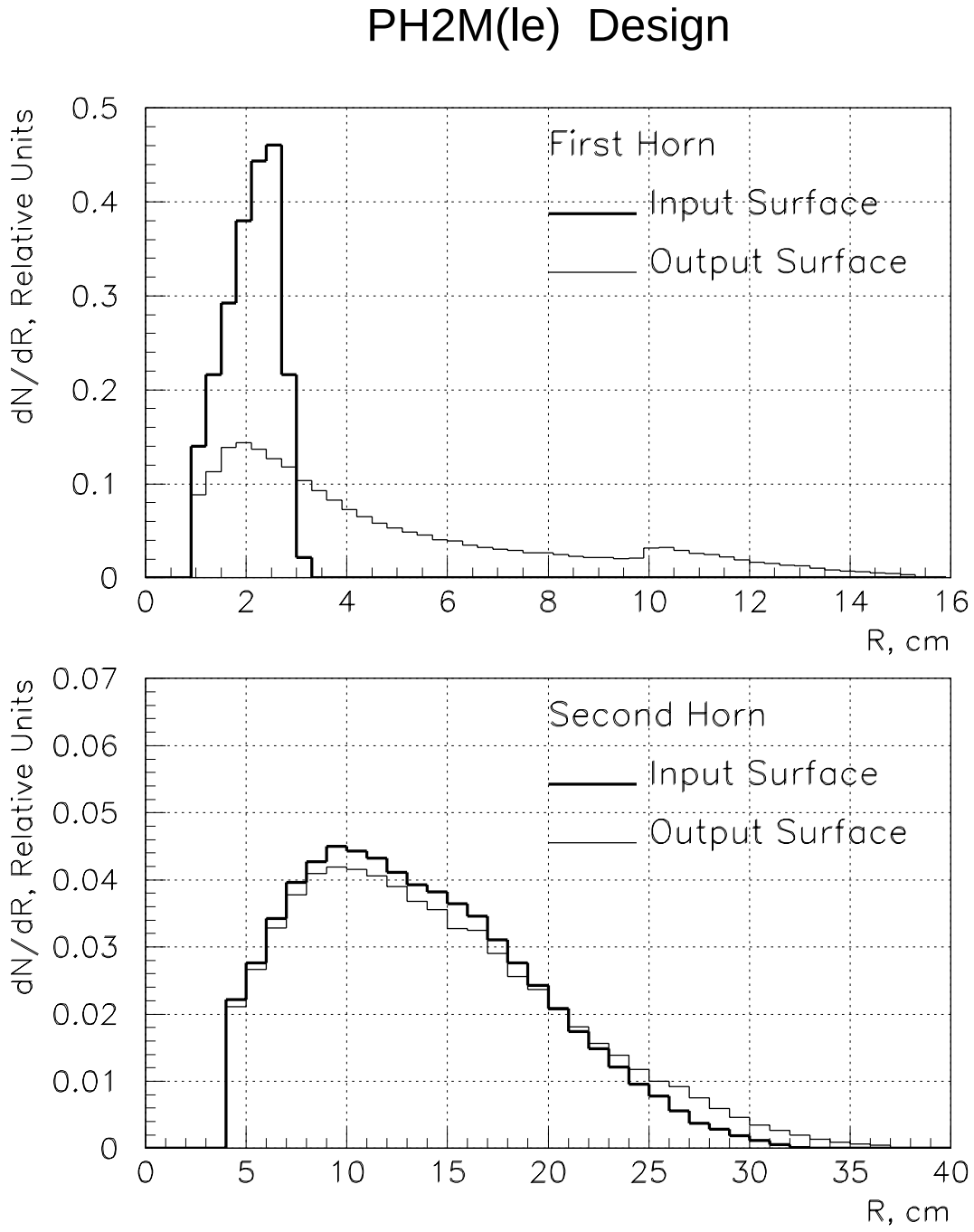

Figure 2.1: The ν_μ CC event rates at the far detector as functions of an inner conductor radius, where pions contributing to this neutrino event rate cross the inner conductor. The LE beam, nominal inner conductor thickness.

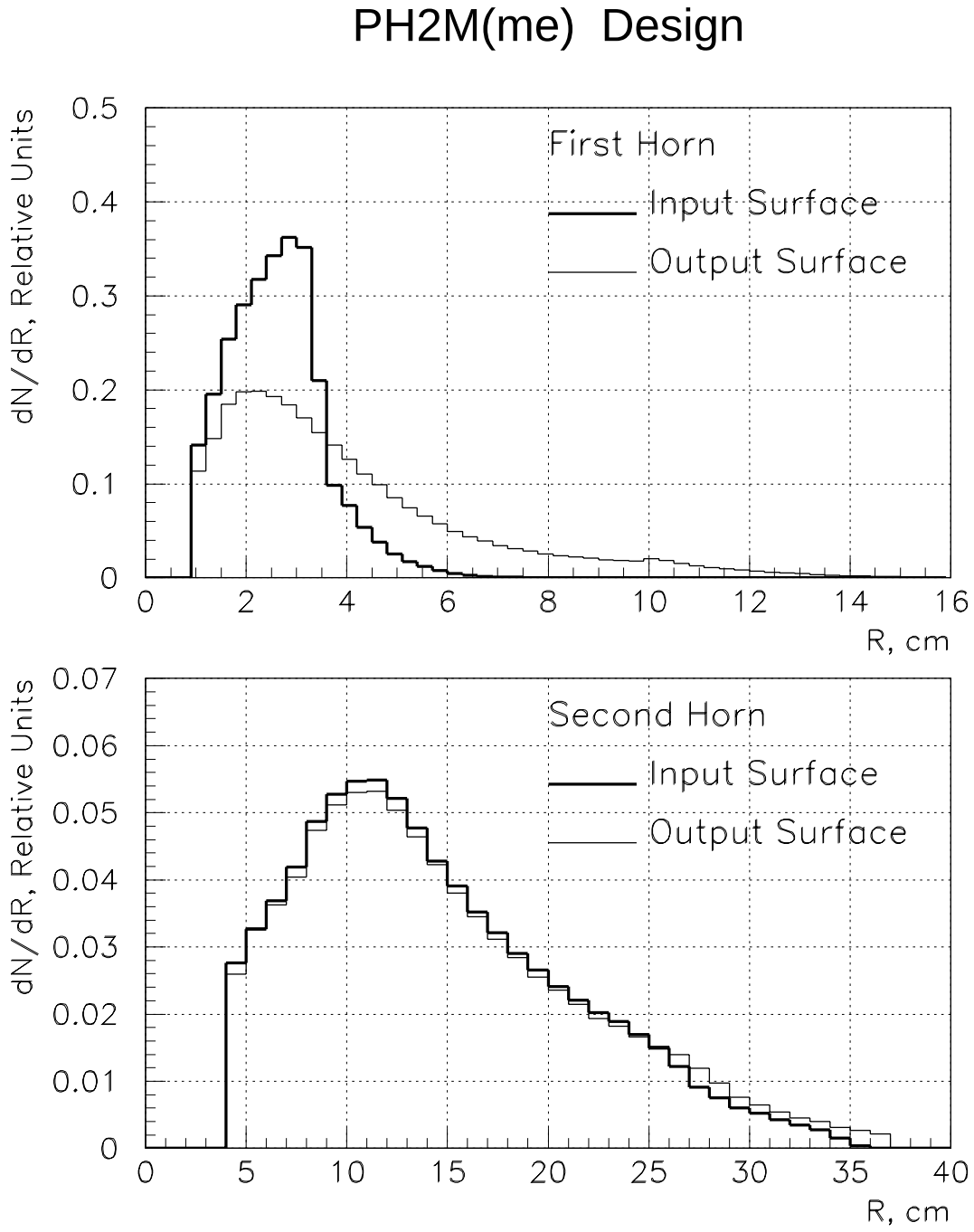

Figure 2.2: The ν_μ CC event rates at the far detector as functions of an inner conductor radius, where pions contributing to this neutrino event rate cross the inner conductor. The ME beam, nominal inner conductor thickness.

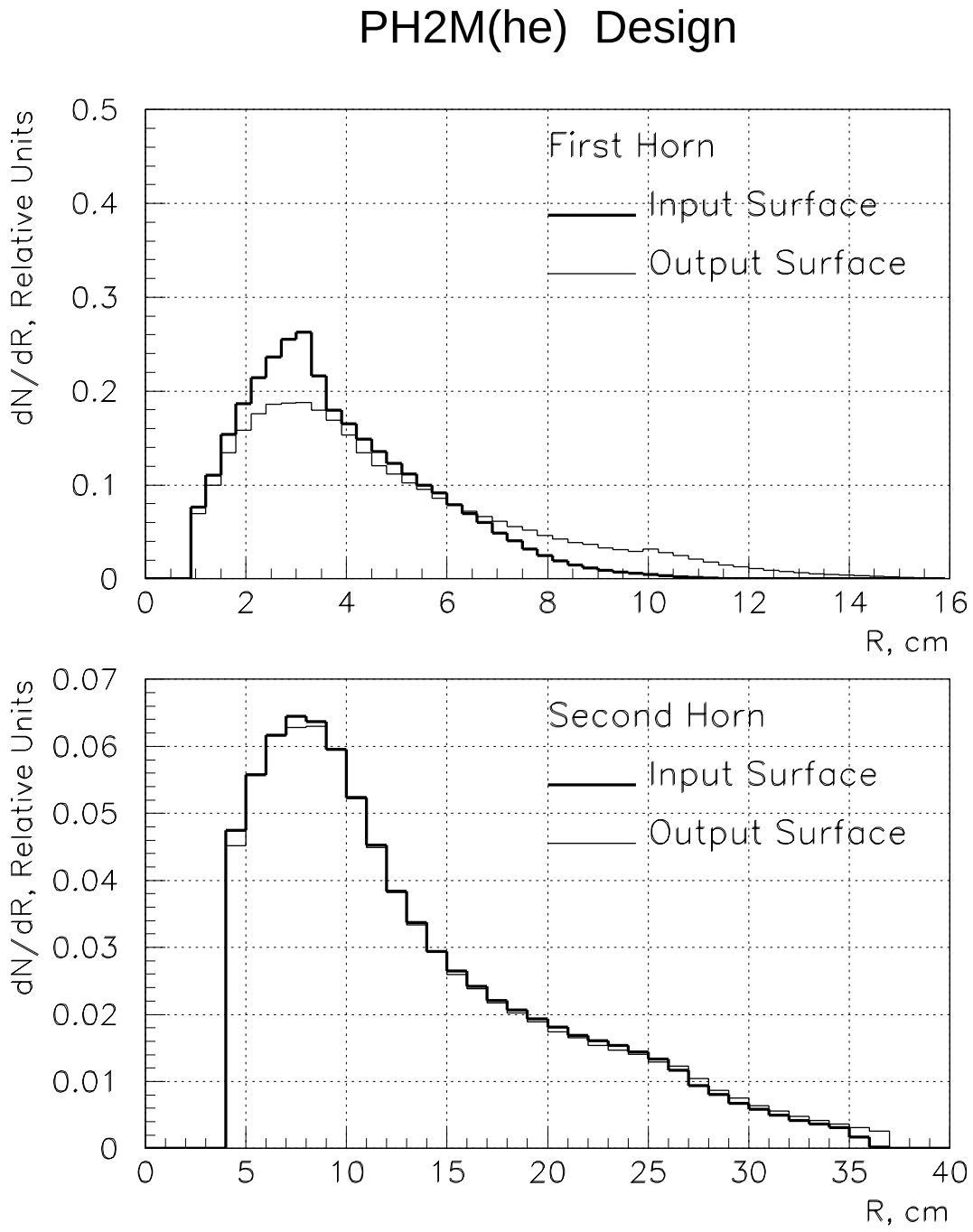

Figure 2.3: The ν_μ CC event rates at the far detector as functions of an inner conductor radius, where pions contributing to this neutrino event rate cross the inner conductor. The HE beam, nominal inner conductor thickness.

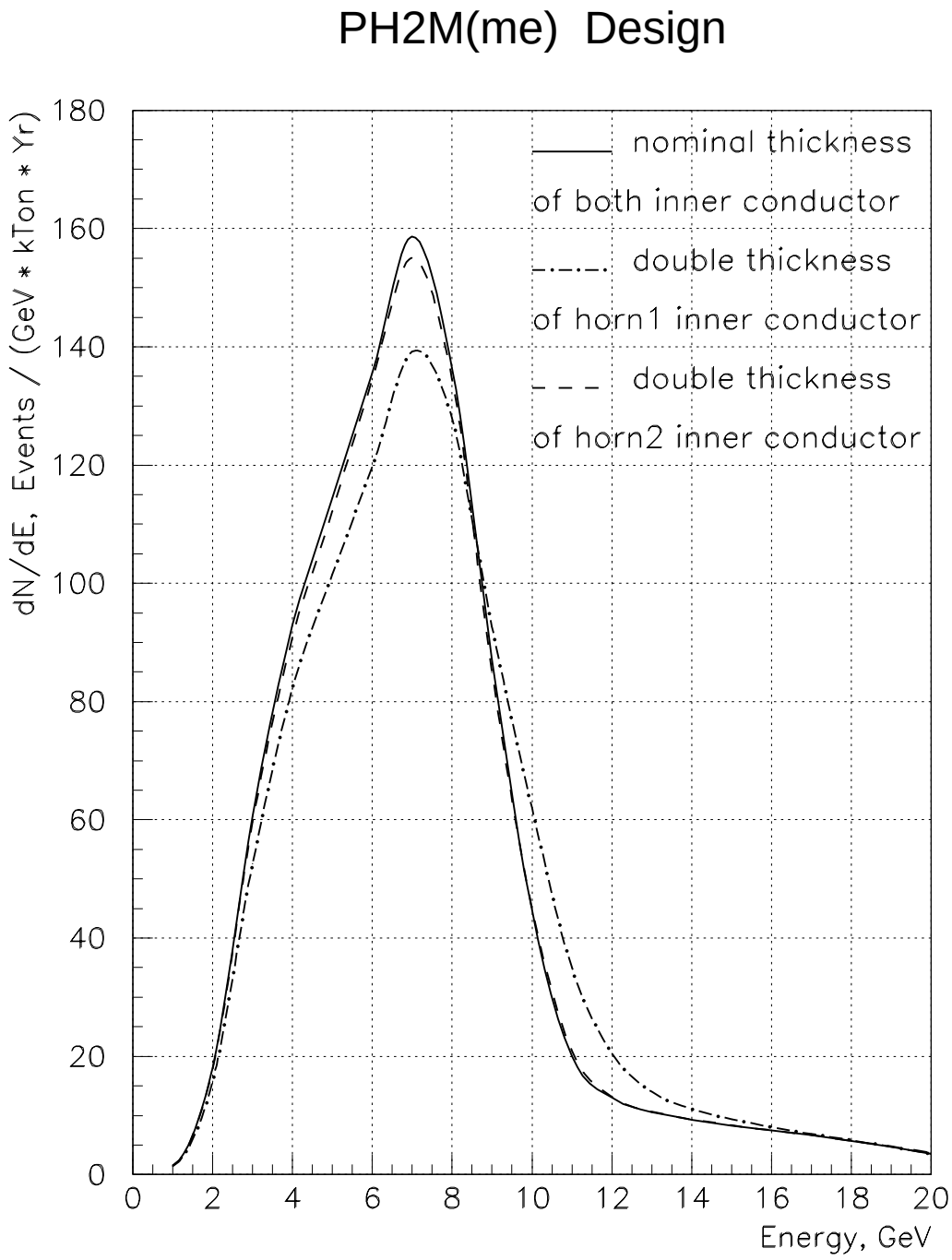

Figure 2.4: Energy spectra of ν_μ CC events at the far detector for the baseline ME beam configuration with double "inside" thicknesses of PH2M horn inner conductors.

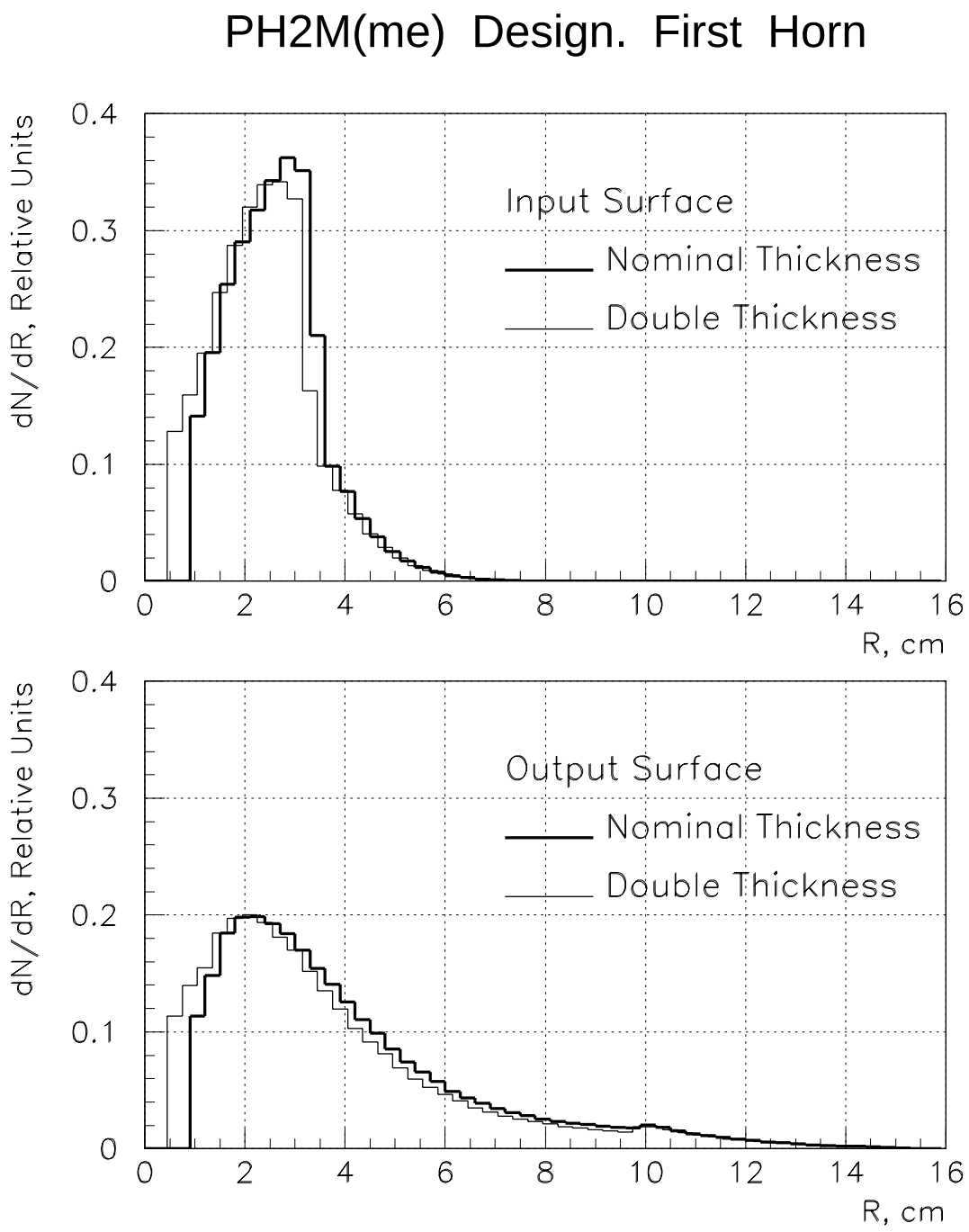

Figure 2.5: The ν_μ CC event rates at the far detector as functions of an inner conductor radius, where pions contributing to this neutrino event rate cross the inner conductor. The ME beam, double "inside" thickness of the inner conductor in the first horn.

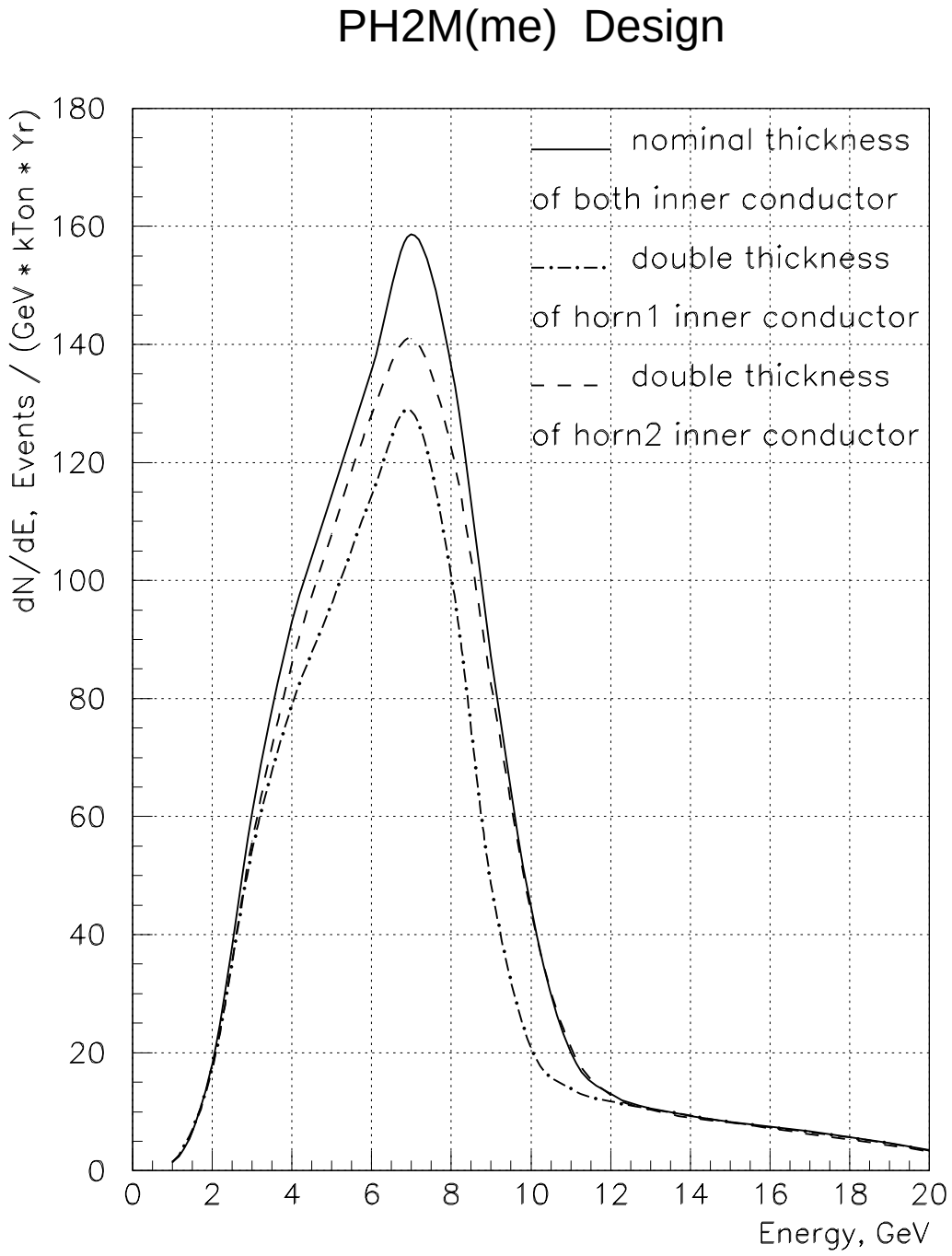

Figure 2.6: Energy spectra of ν_μ CC events at the far detector for the baseline ME beam configuration with double "outside" thicknesses of PH2M horn inner conductors.

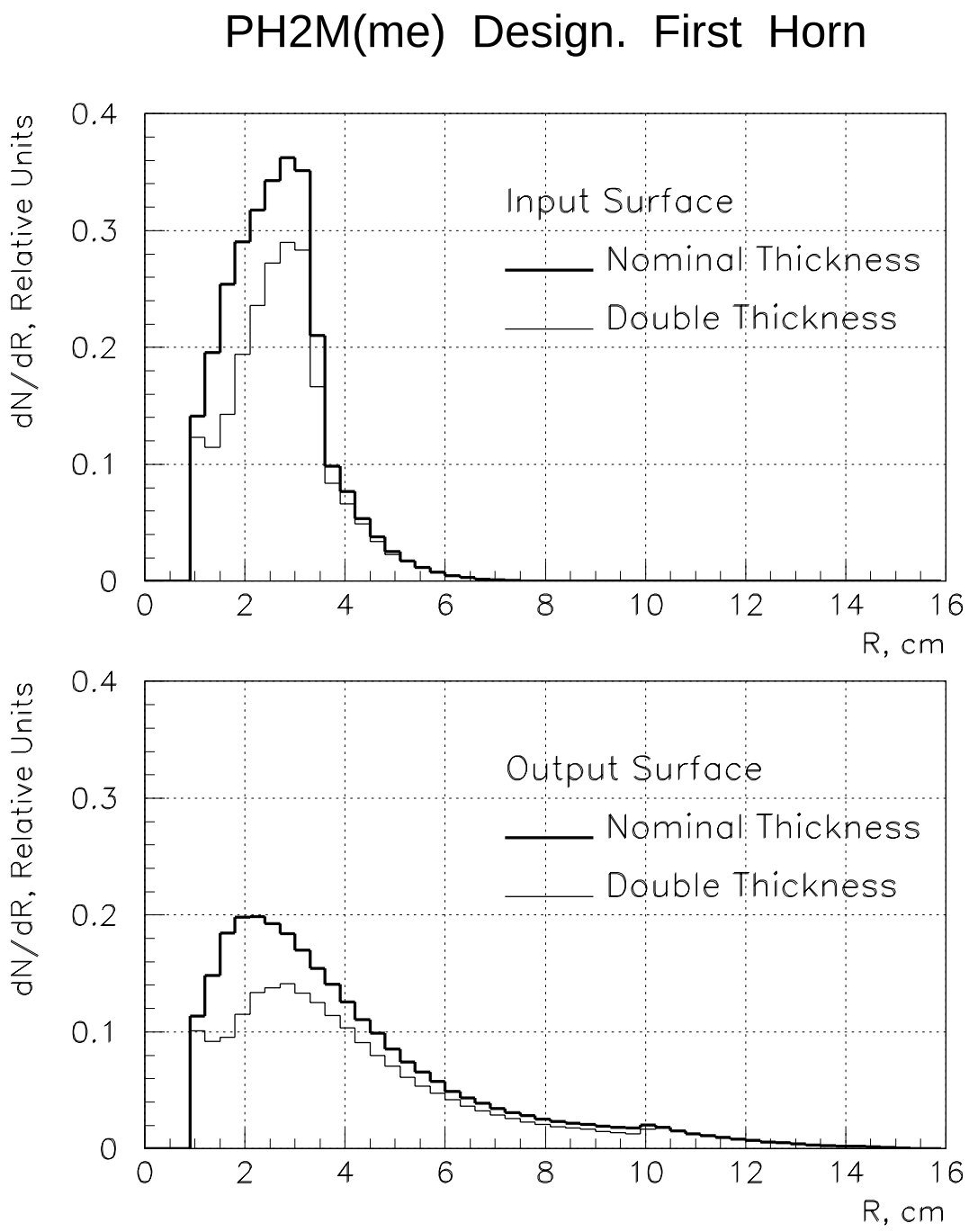

Figure 2.7: The ν_μ CC event rates at the far detector as functions of an inner conductor radius, where pions contributing to this neutrino event rate cross the inner conductor. The ME beam, double "outside" thickness of the inner conductor in the first horn.

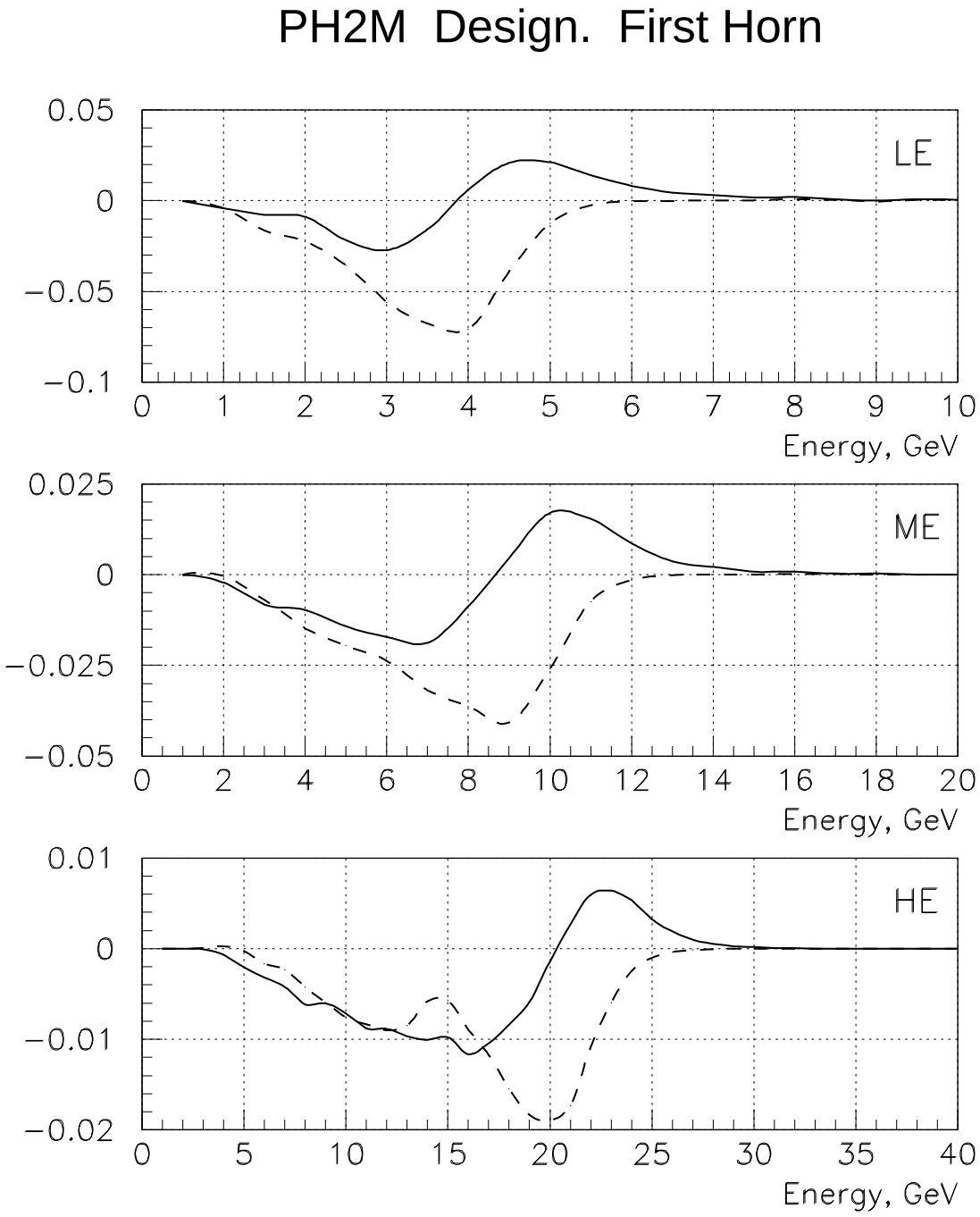

Figure 2.8: Differences between energy spectra of ν_μ CC events at the far detector with double and nominal thicknesses of the inner conductor in the first horn normalized to nominal total event rates $(FAR(t) - FAR(0))/FAR(0)_{total}$. Solid line — double thickness "inside" and dashed line — double thickness "outside".

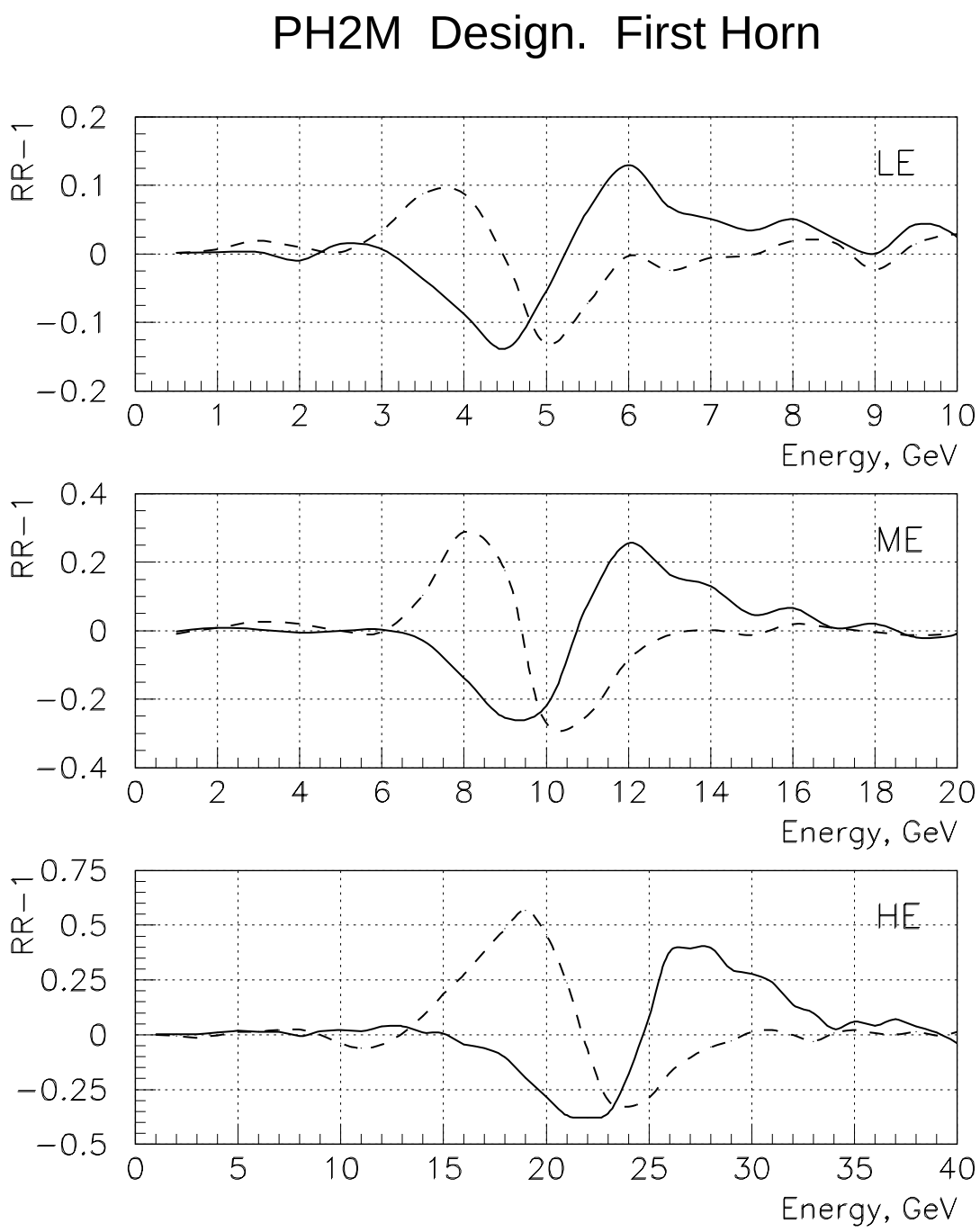

Figure 2.9: RR deviations from 1.0 (see the text) in the case of double thickness of the inner conductor in the first horn. Solid line — the thickness increase "inside" and dashed line — the thickness increase "outside".

3 Horn Construction Tolerances

This Section gives the results of calculations showing the effects of small variations in main sizes of horn inner conductors on neutrino spectra at the far and near detectors. These results may be used for specifying of some horn construction tolerances, although simple models, which have been used in neutrino flux calculations for simulation of the accuracy of inner conductor manufacturing, not always give values for corresponding tolerances directly.

All neutrino flux calculations have been made using the M. C. program HALO for the new PH2M design in the case of the baseline ME beam configuration. Absorption and scattering, as well as focusing of secondaries inside inner conductor walls were taken into account. The 1.2 m long graphite fin target with average density equal to 0.78 of nominal graphite density was used in these neutrino flux calculations.

The effects of variations in main sizes of horn inner conductors on the FAR/NEAR ratio, which will be used to predict the neutrino flux at the far detector, are evaluated here (as in Section 2) by deviation from 1.0 in the worst energy bin of a value of the RR. The 2% level of the RR deviation from 1.0 has been considered as acceptable from the point of view of desirable accuracy of the neutrino flux prediction in the energy range of 0–18 GeV. For the ME beam this energy range contains approximately 90% of the total number of ν_μ CC events at the far detector, moreover, neutrinos with larger energies (high energy tail) may produce backgrounds in some oscillation tests and therefore can be suppressed by a beam plug located downstream the first horn.

3.1 Variations in the Thickness of Horn Inner Conductors

The effects of large variations of inner conductor thicknesses on neutrino spectra for all configurations of the PH2M focusing system have been described in Section 2 and may be used for the optimum choice of the thickness of horn inner conductors during their design (as the compromise between the decrease of absorption losses of secondaries and the increase of mechanical stability of inner conductors). For the baseline ME beam configuration more detailed results are given in Figures 3.1 and 3.2 of this Section, where the effects on neutrino spectra at the far and near detectors and on the

FAR/NEAR ratio, following from an increase of the inner conductor thickness "inside" and "outside" [5], are shown for relatively large values of k in the case when the thickness varies as $t(z) = k * t_0(z)$.

Figure 3.3 shows the RR deviations from 1.0 in the worst energy bin as functions of k for both horns. As it follows from these plots, the acceptable level of 2% in the RR deviation from 1.0 is achieved when the inner conductor thickness in the first horn is increased by a factor of $k \simeq 1.04$. It corresponds to the 0.08 mm increase of the thickness near flanges, where nominal thickness of the inner conductor is equal to 2 mm, and to the 0.18 mm of that in the neck region, where nominal thickness is equal to 4.5 mm. For the second horn the acceptable level of the RR deviation from 1.0 is achieved at substantially larger values of $k \simeq 1.26$–1.46, that corresponds to the 0.5–1.0 mm of an extra material with respect to nominal inner conductor thickness, which is equal here to 2 mm along the whole length of the horn.

The variation of the inner conductor thickness may be also considered as function $t(z) = t_\circ(z) + \Delta t$, where Δt is an invariable value along the horn length. For the first horn Figure 3.4 shows changes in the FAR/NEAR ratio in the case when the thickness increases "outside" in $\Delta t = 1.5$ mm; Figure 3.5 shows the RR deviations from 1.0 in the worst energy bin as functions of Δt.

The $\Delta t = 1.5$ mm increase of the inner conductor thickness leads to somewhat larger changes of the FAR/NEAR ratio than the $k = 1\frac{1}{3}$ thickness increase (Figure 3.4). Taking into account, that the increase of $k = 1\frac{1}{3}$ corresponds to 1.5 mm of an extra material in the neck region and only 0.6 mm of that in the 2.5 m long non–central part of the inner conductor, one should note that the main effect on the FAR/NEAR ratio results from the increase of the thickness in the neck region of the inner conductor. In the case when the thickness increase is the same along the length, the acceptable level of 2% in the RR deviation from 1.0 is achieved for the first horn at $\Delta t \simeq 0.13$ mm, as it follows from Figure 3.5.

Due to a linear dependence of the RR deviation from 1.0 for small values of k and Δt, the same results may be expected also in the case of the small decrease of the inner conductor thickness.

[5] The difference between increasing of the inner conductor thickness "inside" and "outside" was explained in Section 2.

3.2 Variations in the Distance Between Upstream and Downstream Horn Parabolas

The increase of the inner conductor thickness "outside" leads to the decrease of a distance between the upstream and downstream horn parabolas. For given radius r changing of the distance between two parabolas may be estimated as: $\Delta L = -2(p_u + p_d) r \Delta t$, where p_u and p_d are parameters of the upstream and downstream parabolas respectively. Thus, for the first horn with $p_u = 7.05$ cm^{-1} and $p_d = 2.19$ cm^{-1} (see Table 1.1), $\Delta t = 0.13$ mm (the increase of the thickness is invariable along the horn) gives the shortening of the distance between two parabolas by the value of $\Delta L \approx 3.5$ mm at $r = 1.5$ cm (neck region) and twice as more at $r = 3.0$ cm. Because the main effect on the FAR/NEAR ratio provides the change of inner conductor parameters in the neck region, the tolerance on the distance between two parabolas of the inner conductor in the first horn may be estimated by the value of ≤ 3.5 mm.

On the other hand, the variation of a distance between two parabolas with nominal thicknesses causes simultaneous changes in the shape and position of two inner conductor surfaces, which will increase the deviation of the RR with respect to the case of the thickness increase "outside" only and consequently will increase a request to the tolerance on the distance between two parabolas. Figure 3.6 gives results of calculations showing the effect of ΔL variations in each horn on the FAR/NEAR ratio. As it follows from these plots, the acceptable level of the RR deviation from 1.0 is achieved at $|\Delta L| \approx 2$ mm and $|\Delta L| \approx 3.5$ mm for the first and second horns respectively.

One should note, that behavior of the FAR/NEAR ratio in the case of variations of a distance between two parabolas are similar to those in the case of variations in the inner conductor thickness (see Figure 3.1 and 3.2).

3.3 The Eccentricity Between Inner and Outer Surfaces of Inner Conductors

The results given here show the effects of mutual displacement of inner and outer surfaces (eccentricity) of inner conductors in both horns on neutrino spectra. In our M.C. simulations of the effects of an eccentricity on neutrino spectra we suppose, that at the given longitudinal position Z of the parent

mesons the magnetic field produced by the inner conductor coincide in the first approach with the magnetic field of the infinite conductor with $r_1 = R_{in}^{IC}(Z)$ and $r_2 = R_{out}^{IC}(Z)$ and δ, as it is shown below.

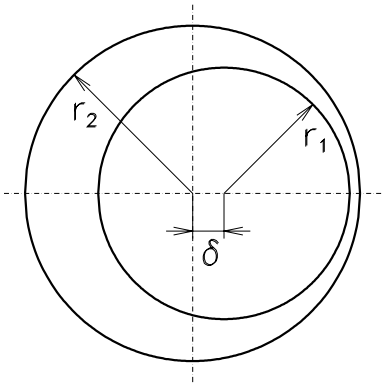

In this case, the magnetic field at the each point inside and outside of inner conductor walls may be defined as superposition of magnetic fields produced by two currents with constant density $j = I/\pi(r_2^2 - r_1^2)$ flowing in opposite directions along infinite cylindrical conductors. The internal and external magnetic fields in each conductors are:

$$B_{in} = \frac{\mu_0 j}{2} r, \qquad B_{ex} = \frac{\mu_0 j}{2} \frac{r_{1(2)}^2}{r},$$

where r is the distance between the axis of the corresponding conductor and the point (x, y) where the field is calculated ($r^2 = (x - \delta)^2 + y^2$ for dislodged conductor and $r^2 = x^2 + y^2$ for non-dislodged one).

The eccentricity δ leads to changes of the magnetic field distribution inside and outside of inner conductor walls, in particular the dipole field $B_y \sim \delta$ appears in the area of $r \leq R_{in}^{IC}$ initially free from the magnetic field. It so happened that this dipole field gives the main contribution (~85%) in the deviation of the FAR/NEAR ratio from its nominal value. In the area between the inner and outer conductors an eccentricity δ adds some corrections in the focusing field $B_0 \sim 1/r$:

$$\frac{\Delta B_\phi}{B_0} = -\frac{r_1^2}{r_2^2 - r_1^2} \cdot \frac{\delta}{r} \cos\phi, \qquad \frac{B_r}{B_0} = \frac{r_1^2}{r_2^2 - r_1^2} \cdot \frac{\delta}{r} \sin\phi.$$

Figures 3.7 and 3.8 show the effects of an eccentricity invariable along the inner conductor length on neutrino spectra at far and near detectors and on the FAR/NEAR ratio. As it follows from these plots, the acceptable level of 2% in the RR deviation from 1.0 is achieved at the $\delta \simeq 0.035$ mm and $\delta \simeq 0.07$ mm for the first and second horns respectively.

The model with an eccentricity invariable along the length looks as not quite real from the point of view of the horn conductors fabrication, which assumes welding together of 3–4 separately produced pieces of the inner conductor. In this case one may expects not so strong tolerances for the eccentricity of inner conductor surfaces. Points 1 and 2 in Figure 3.8 show

results of calculations for horns 1 and 2, when the inner conductor of each horn consists of two parts (from the upstream end to the neck and from the neck to the downstream end) with the eccentricity of $\delta = +0.2$ mm in the first part and $\delta = -0.2$ mm in the second one. In this case, as it follows from Figure 3.8, deviations of RR from 1.0 decreased approximately by the factor of 3.6 and 2.8 for the first and second horns respectively.

3.4 The Ellipticity of Inner and Outer Surfaces of Inner Conductors

The effects on neutrino spectra at the far and near detectors are given below for small elliptical deviations of inner conductor surfaces from their circular shapes. The magnetic field inside and outside of non–circular inner conductor walls has been calculated as superposition of magnetic fields produced by two currents with constant density $j = I/\pi(r_2^2 - r_1^2)$ flowing in opposite directions along infinite cylindrical and elliptical conductors in which transversal sizes coincide in each longitudinal position with those for the inner conductor.

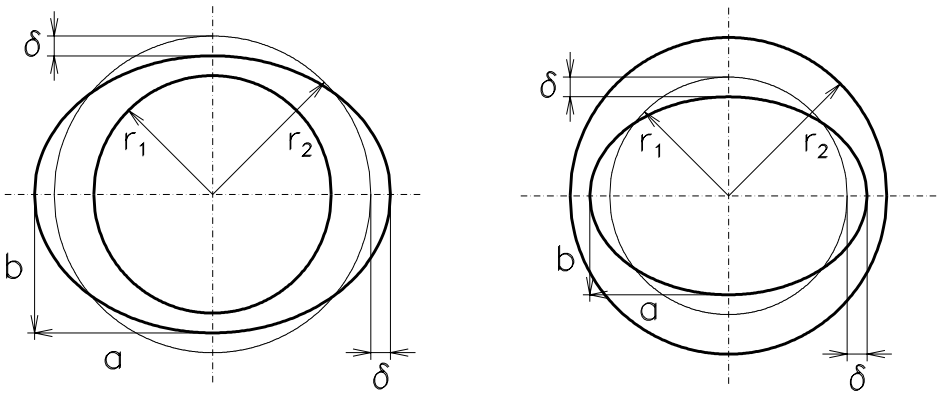

The internal and external magnetic fields of the infinite elliptical conductor with semi-axis a and b produced by the current with constant density j can be evaluated as [6]:

$$B_{in} = B_y + iB_x = \frac{\mu_0 j}{a+b}(bx - iay),$$

[6] R.A.Beth, Proc. of 1968 Summer Study on Superconducting Devices, Report BNL 50155, v.3, p.843.

$$B_{ex} = \frac{\mu_0 j a b}{z + \sqrt{z^2 - c^2}},$$

where $z = x + iy$ is a coordinate of the point where the field is calculated and $c^2 = a^2 - b^2$.

Some changes in the magnetic field distribution, which appear around inner conductor walls due to the ellipticity of inner conductor surfaces, i.e. the quadrupole field with gradient $G \sim \delta$ in the area of $r \leq R_{in}^{IC}$ and more rapid decreasing with radius variations in the focusing field between the inner and outer conductors

$$\frac{\Delta B_\phi}{B_0} = \mp \frac{r_{1(2)}^2}{r_2^2 - r_1^2} \cdot \frac{r_{1(2)}\delta}{r^2} \cos 2\phi, \qquad \frac{B_r}{B_0} = \pm \frac{r_{1(2)}^2}{r_2^2 - r_1^2} \cdot \frac{r_{1(2)}\delta}{r^2} \sin 2\phi.$$

are not so dangerous for the stability of the FAR/NEAR ratio as those in the case of the inner conductor eccentricity. As for the eccentricity of inner conductors, the main effect on neutrino spectra gives here the appearance of the magnetic field in the region of $r \leq R_{in}^{IC}$.

Figure 3.9 illustrates the effects of the $\delta = 0.4$ mm ellipticity of the inner conductor in the first horn on neutrino spectra and on the FAR/NEAR ratio, while Figure 3.10 gives the dependence of the RR deviation from 1.0 on the inner conductor ellipticity in both horns (all plots are given for the ellipticity of the inner conductor invariable along the horn length). In fact, the influence on neutrino spectra of the ellipticity is rather smaller than that in the case of eccentricity of the inner conductor, as well as the difference between influences of the ellipticity in the first and second horns. The acceptable level of 2% in the RR deviation from 1.0 is achieved at $\delta \sim 0.1$ mm and $\delta \sim 0.2$ mm for the first and second horns respectively.

3.5 Conclusions

Within simple models, which have been used here for M.C. simulations of the effects of variations in main sizes of inner conductors on the FAR/NEAR ratio, the corresponding construction tolerances for inner conductors in PH2M horns can be determined as those which are given in Table 3.1.

As it follows from these results, the effects on the FAR/NEAR ratio of all considered in this Report variations of the inner conductor sizes are substantially different for the first and second horns, i.e. the construction

tolerances for the second horn may be approximately factor 2 lower than those for the first horn.

Variations of inner conductor sizes	Horn#1	Horn#2
Invariable along the length thickness change	0.13 mm	0.25 mm
Distance between inner conductor parabolas	2.0 mm	3.5 mm
Invariable along the length eccentricity of the inner conductor	0.035 mm	0.070 mm
Invariable along the length ellipticity of the inner conductor	0.12 mm	0.18 mm

Table 3.1: The values of variations in main sizes of inner conductors, which will cause the 2% deviation of the RR from 1.0.

One should note also, that for horns which consist of some separately fabricated and then welded together parts:

- the high accuracy of the inner conductor radii R_{in}^{IC} and R_{out}^{IC} (and correspondingly of the inner conductor thickness) is very important for the relatively short (~0.5 m) central part of the inner conductor in its neck region, while the same accuracy for the upstream and downstream parts of inner conductor may be much more lower. Figures 3.1, 3.2 and 3.4 show negligible deviation of the RR from 1.0 for neutrinos with $E_\nu \leq 6$ GeV, which appear from secondaries crossing inner conductor walls mainly through these non–central parts of the inner conductor;
- the construction tolerances for the inner conductor eccentricity and ellipticity may be not so high as they are given in Table 3.1. Figure 3.8 shows a simple example illustrating a substantial decrease of the RR deviation from 1.0 in the case when inner conductors in both horns consist of two parts with equal and opposite directed eccentricities.

The evaluation of these tolerances for horns fabricated from some separately produced pieces may be done taking into account a partial effects of variations of main sizes in the each part of inner conductors on the FAR/NEAR ratio.

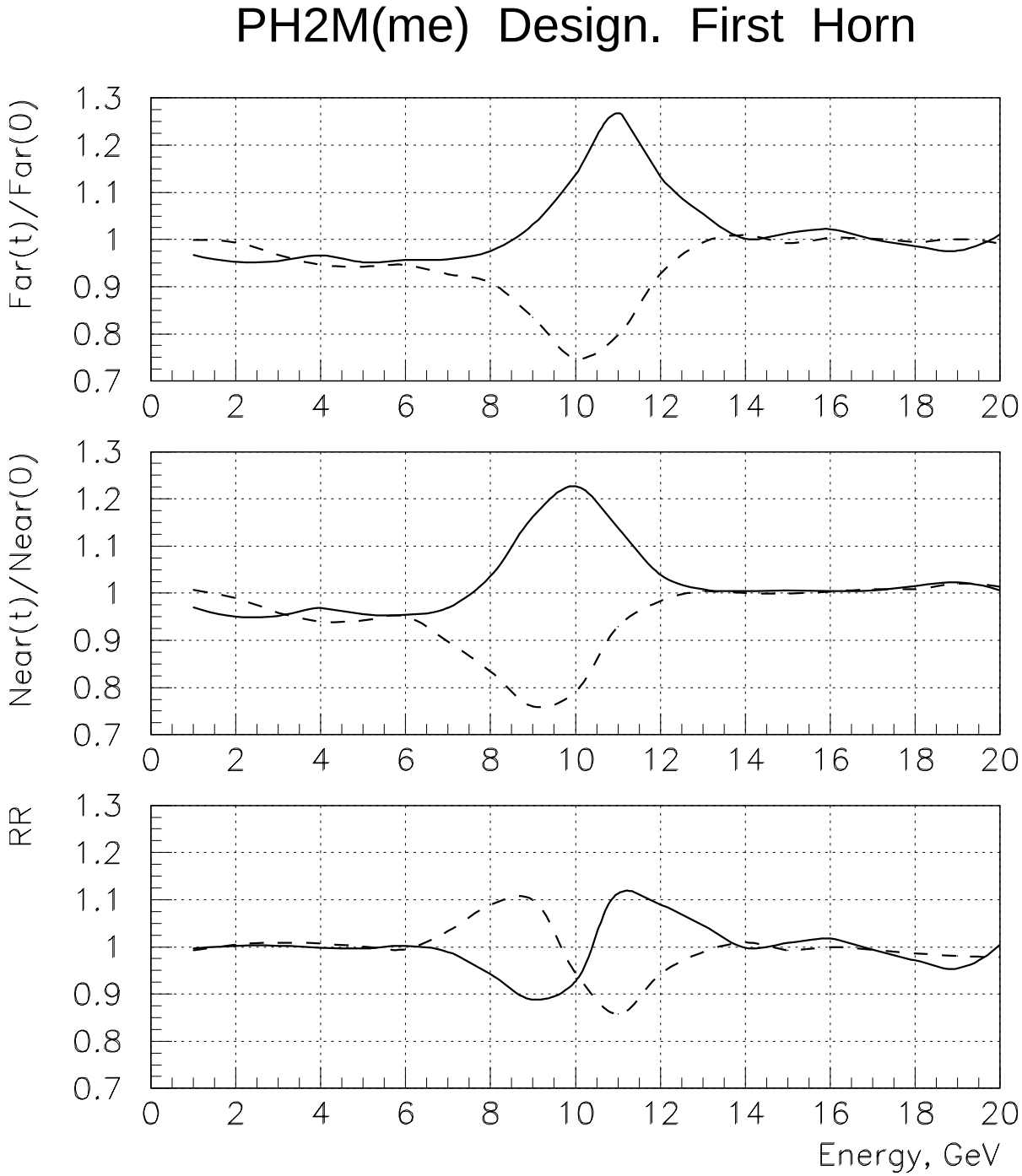

Figure 3.1: The effects of the $k = 1\frac{1}{3}$ thickness increase of the inner conductor in the first horn on the far detector flux (top), near detector flux (middle) and FAR/NEAR ratio (bottom). Solid line — the thickness increase "inside" and dashed line — the thickness increase "outside".

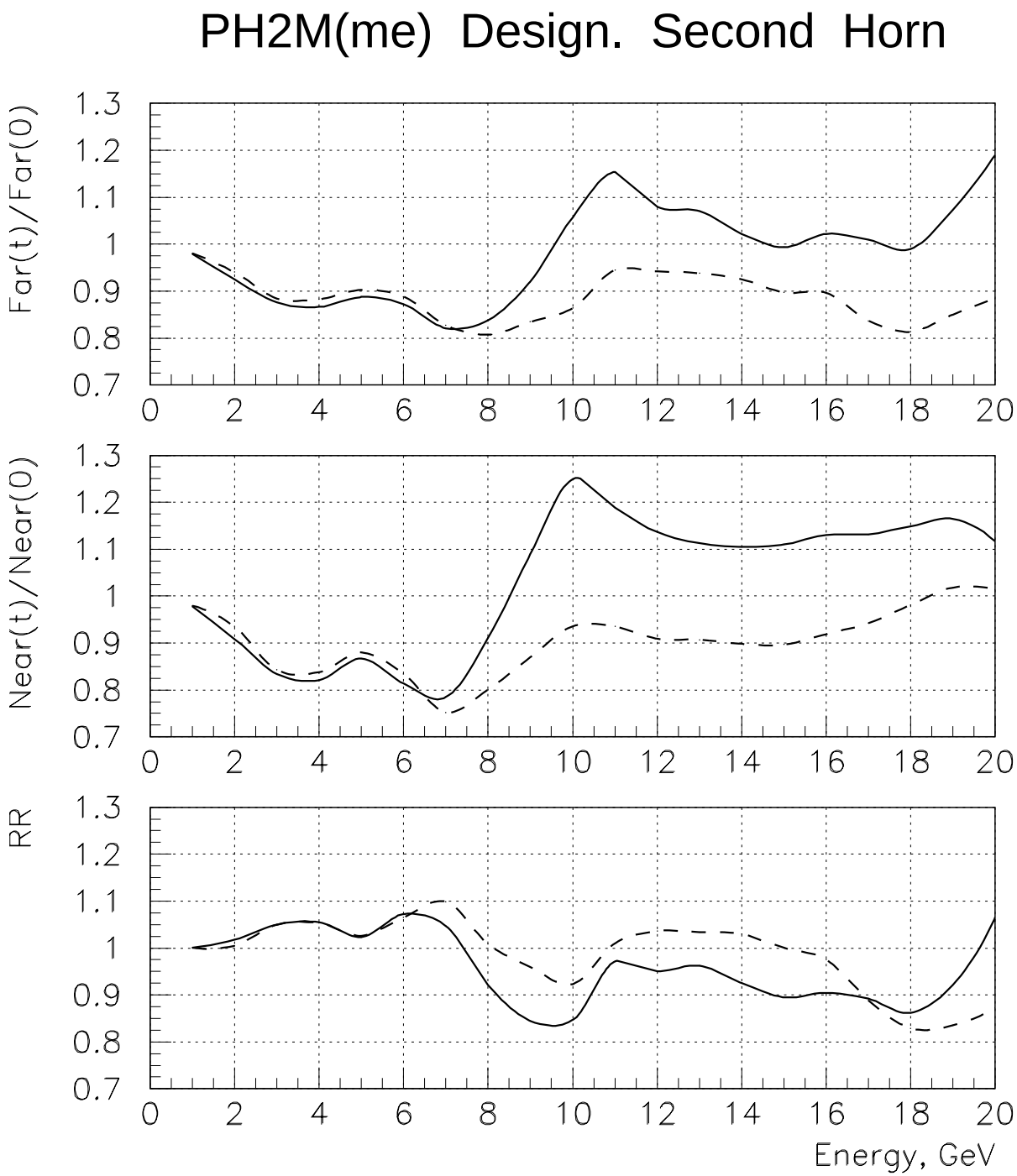

Figure 3.2: The effects of the $k = 4$ thickness increase of the inner conductor in the second horn on the far detector flux (top), near detector flux (middle) and FAR/NEAR ratio (bottom). Solid line — the thickness increase "inside" and dashed line — the thickness increase "outside".

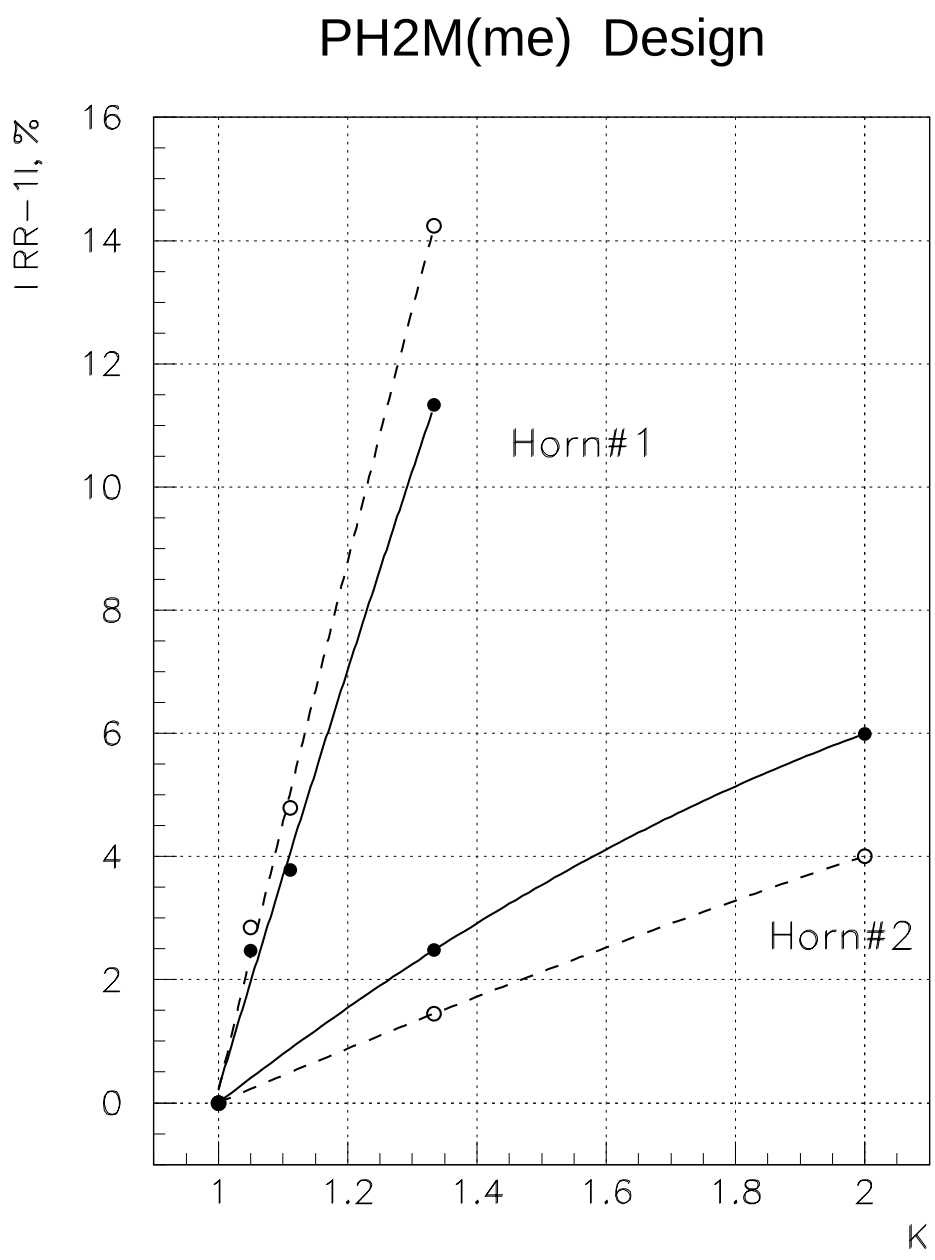

Figure 3.3: RR deviations from 1.0 in the worst energy bin as functions of the increase (k) of the inner conductor thickness. Solid line — the thickness increase "inside" and dashed line — the thickness increase "outside".

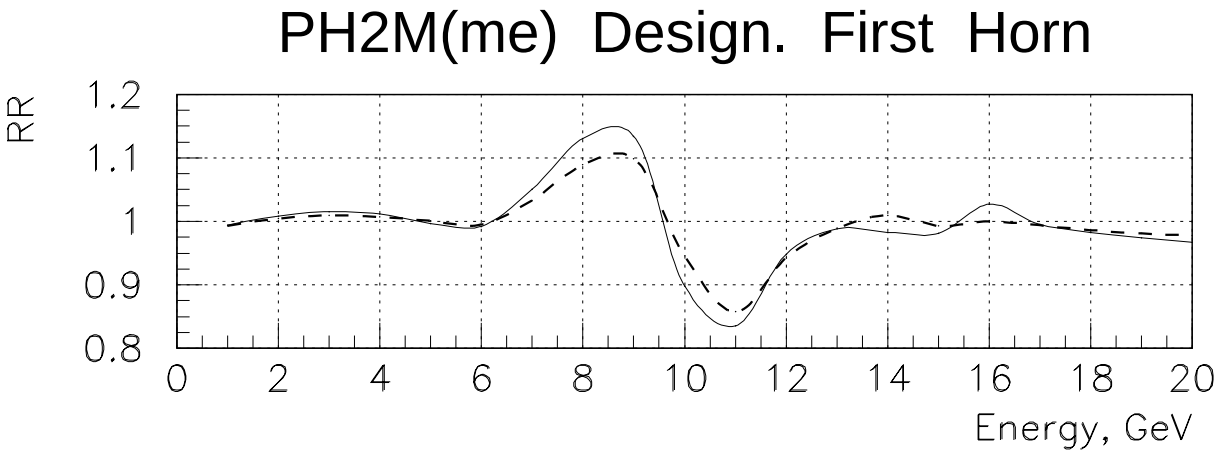

Figure 3.4: The effect of the increase "outside" of the inner conductor thickness in the first horn on the FAR/NEAR ratio. Solid line — the thickness increase on the value of $\Delta t = 1.5$ mm and dashed line — the $k = 1\frac{1}{3}$ thickness increase.

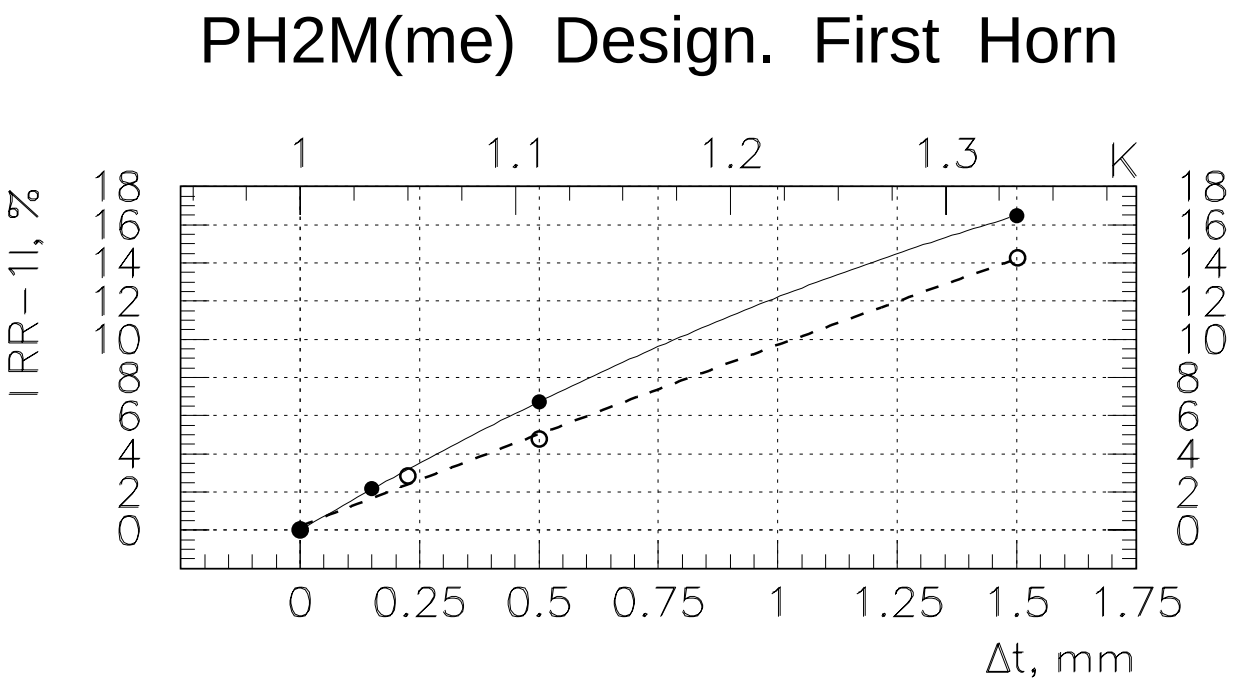

Figure 3.5: RR deviations from 1.0 in the worst energy bin as functions of the increase of the inner conductor thickness in the first horn. Solid line — the thickness increase on the value of Δt and dashed line — the factor k thickness increase.

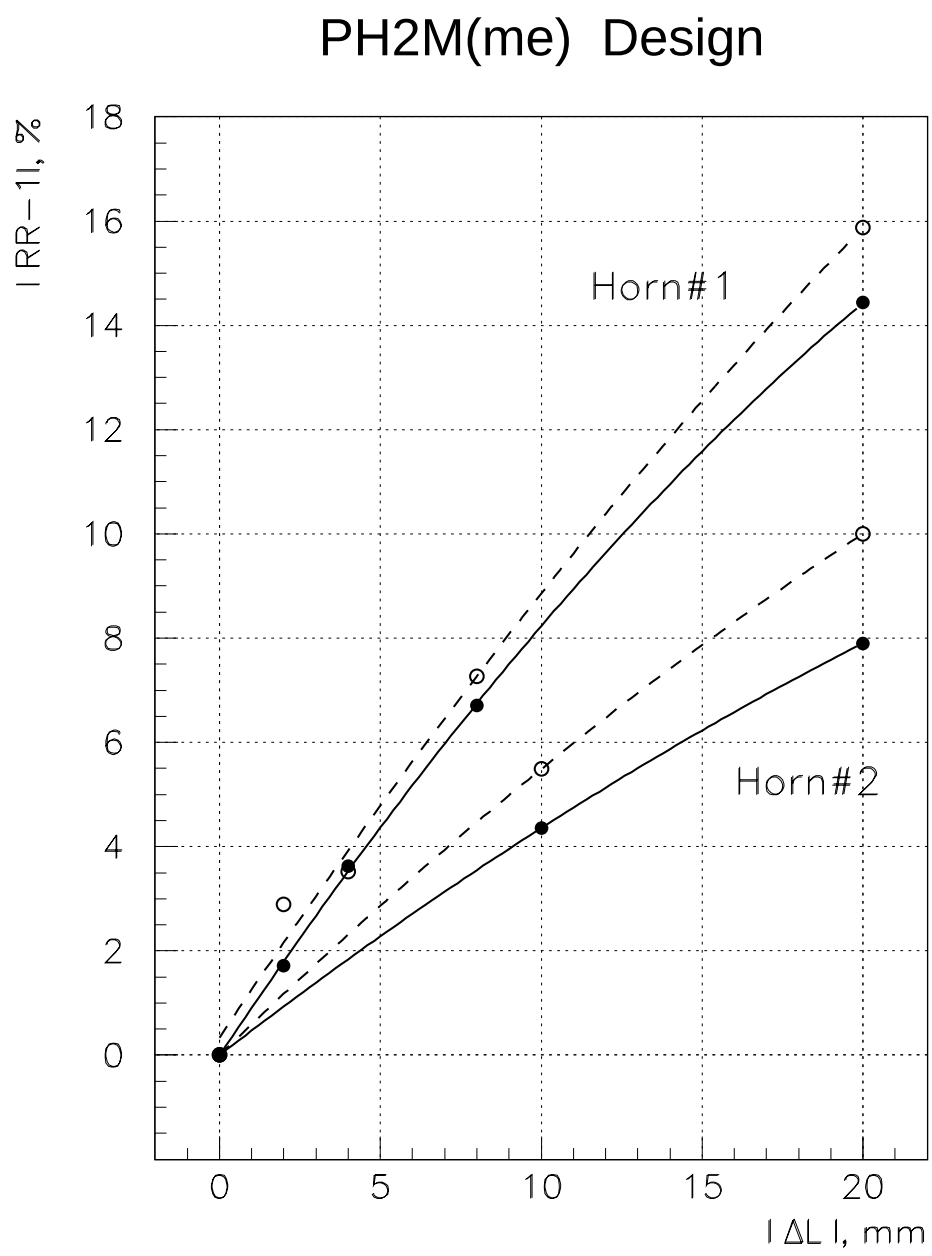

Figure 3.6: RR deviations from 1.0 in the worst energy bin as functions of the distance between two parabolas of the inner conductor. Solid line — for $\Delta L \geq 0$ and dashed line — $\Delta L \leq 0$.

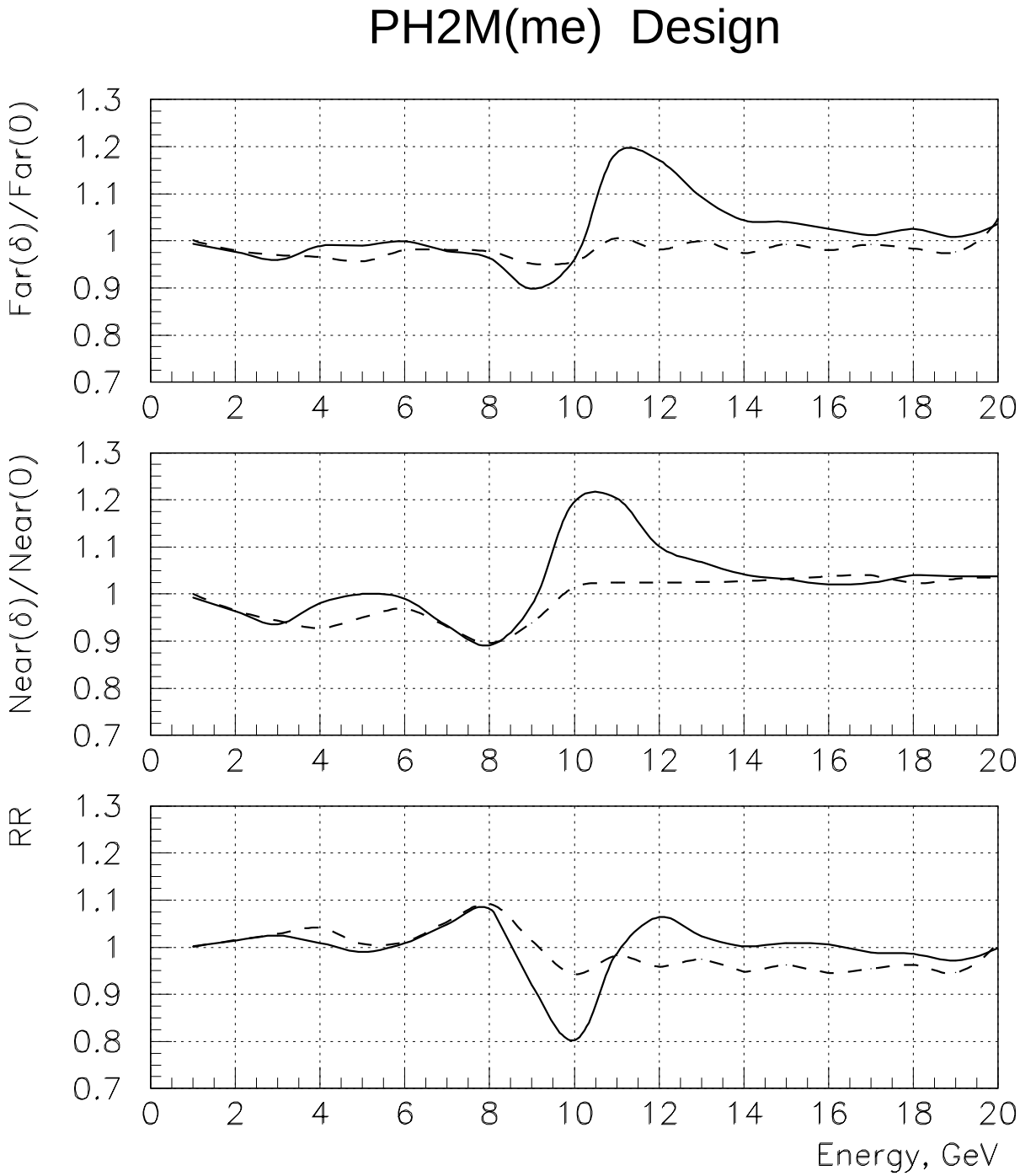

Figure 3.7: The effects of the $\delta = 0.2$ mm eccentricity between inner and outer surfaces of inner conductors on the far detector flux (top), near detector flux (middle) and FAR/NEAR ratio (bottom). Solid line — in the first horn and dashed line — in the second horn.

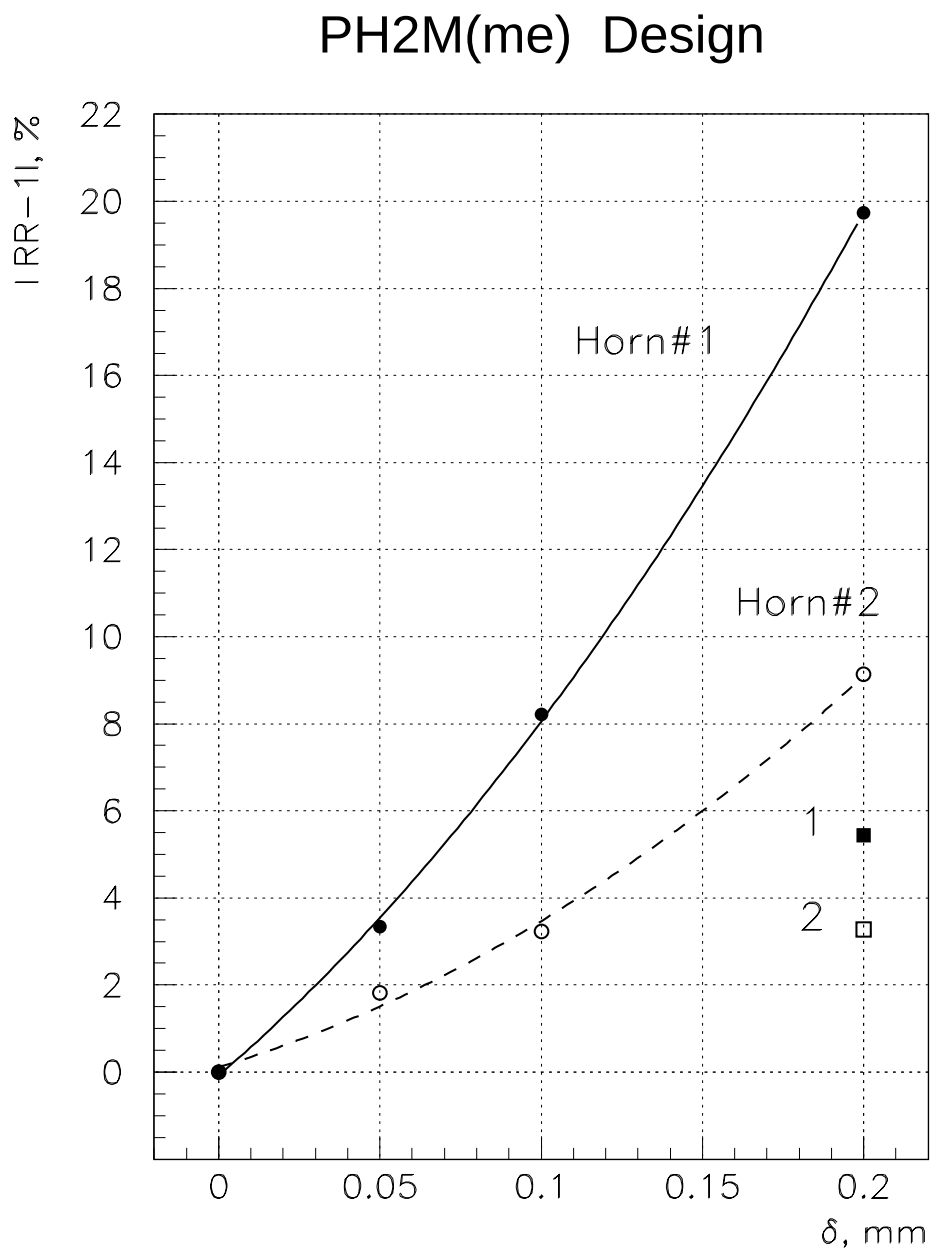

Figure 3.8: RR deviations from 1.0 in the worst energy bin as functions of the eccentricity between inner and outer surfaces of inner conductors. Points 1 and 2 are explained in the text.

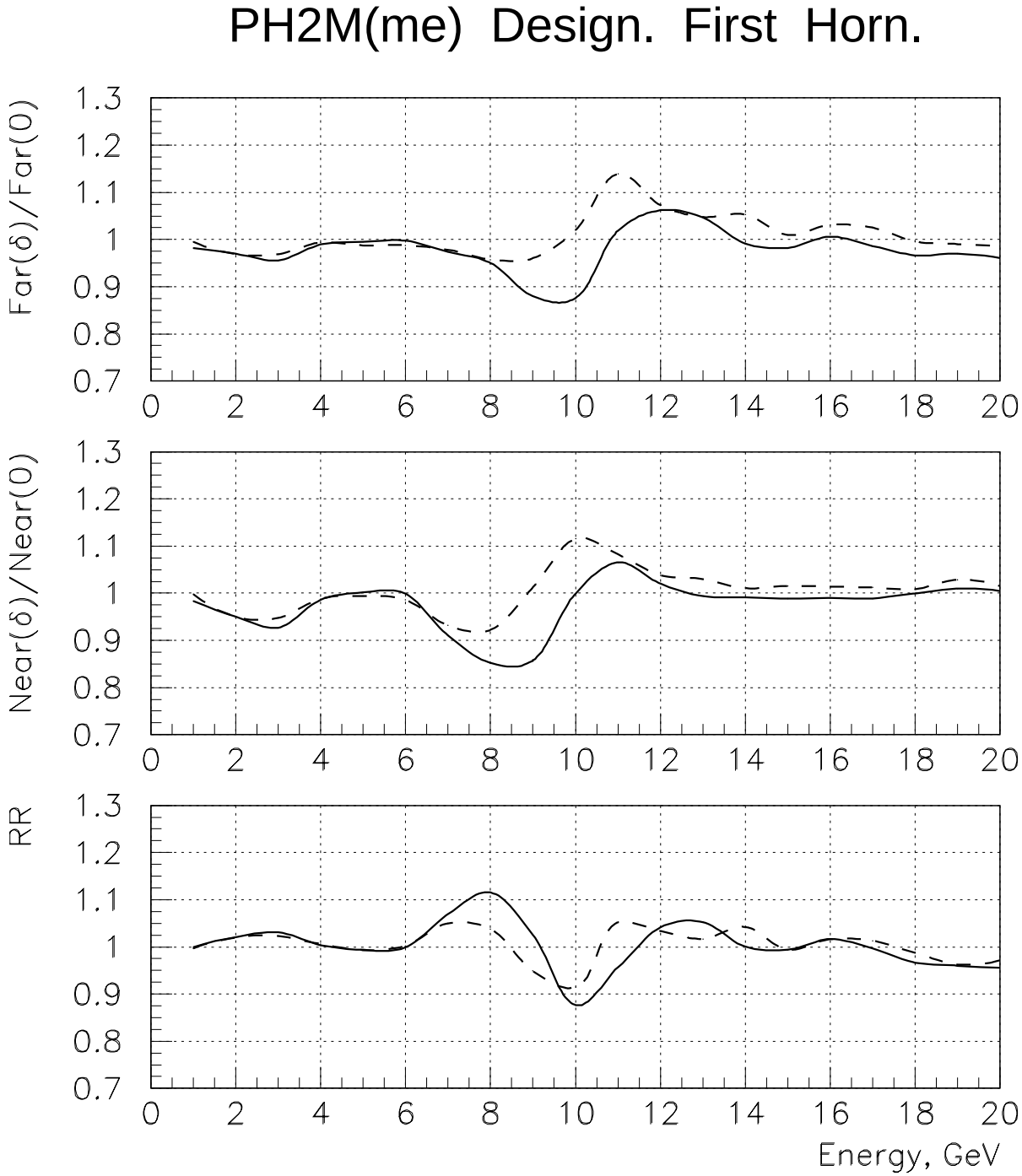

Figure 3.9: The effects of the $\delta = 0.4$ mm ellipticity of the inner conductor in the first horn on the far detector flux (top), near detector flux (middle) and FAR/NEAR ratio (bottom). Solid line — the ellipticity of the outer surface and dashed line — the ellipticity of the inner surface.

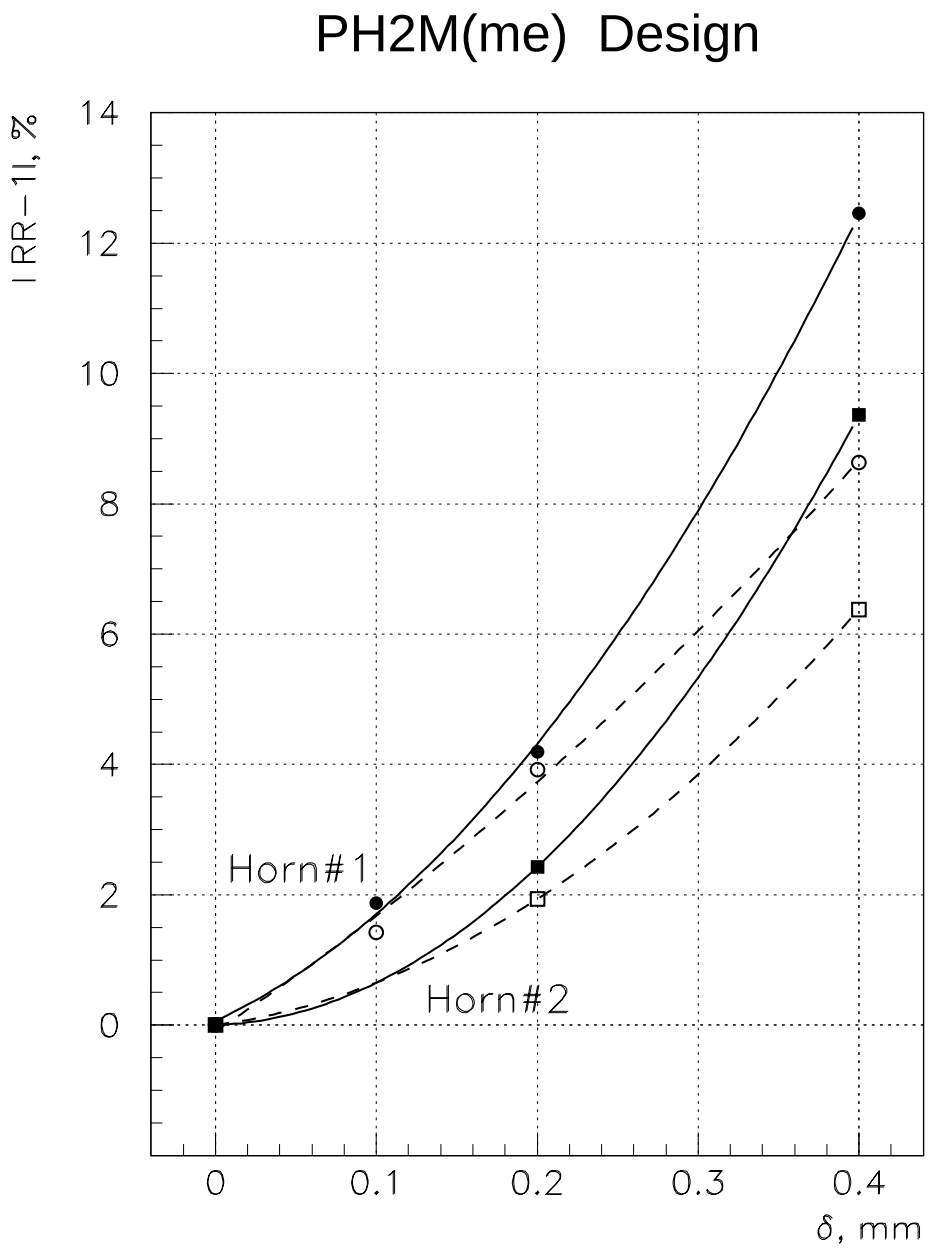

Figure 3.10: RR deviations from 1.0 in the worst energy bin as functions of the ellipticity of inner conductors. Solid line — the outer surface ellipticity and dashed line — the inner surface ellipticity.